

Enhancement of fast scan cyclic voltammetry detection of dopamine with tryptophan

Sarah Elizabeth Thompson

A Thesis Submitted to the Graduate Faculty of

GRAND VALLEY STATE UNIVERSITY

In

Partial Fulfillment of the Requirements

For the Degree of

Master of Science

Cell and Molecular Biology

April 2018

Dedication

My thesis is dedicated to my grandmother, Sharon Thompson, who passed away before I was able to finish writing this. In her life, she was one of my biggest supporters. Near the end of her life she developed Alzheimer's disease, a cruel and unjust disease which drastically affected her condition of life. Although she is gone, her love and support for me is not forgotten, and continues to drive me to pursue my scientific goals. Thank you, nana.

Acknowledgements

First and foremost, I would like to thank my committee chair and advisor, Dr. Ramsson, for seeing potential in me as a student, and guiding me throughout this research journey. From him, I have learned how to communicate, troubleshoot, and how to remain positive when under stress. I would like to thank Dr. Khoo for advising me, and helping me to grow as a scientist in the professional world. As well, I would like to thank Dr. Thorgaard for his expertise and helping me to understand electrochemical principles imperative to my research which lie outside the realm of cell and molecular biology. Thank you also to Dr. Korich for the experimental compounds which inspired this project.

Special thanks to my parents, for their continued love and support during my extended academic career. Lastly, I would like to say thank you to my loving fiancé, Jordan. Your patience and unwavering support served as the cornerstone for my strength and stability during my research. You spent many nights listening to me discuss my research and dilemmas in detail, despite not understanding any of it. I am truly grateful for your constant encouragement as I pursue my academic goals.

Abstract

Dysregulation of dopamine release is a pathological effect of common neurodegenerative diseases, including Alzheimer's disease and Parkinson's disease. Fast scan cyclic voltammetry (FSCV) has been used as an analytical tool to investigate the role of dopamine in these diseases, and in relation to drug addiction and reward behavior. Methods to improve the sensitivity of FSCV have involved modifying the surface of the carbon electrodes used for dopamine detection, altering the potential waveform, and changing the structure of the carbon sensor. Here, the amino acid tryptophan was investigated as a potential surface modification for increased dopamine detection. This study serves as an *in vitro* proof of concept for tryptophan modified electrodes for FSCV detection of dopamine. The mechanism of tryptophan surface modification was also investigated in this study. Tryptophan covalently binds to the carbon surface at the 3' nitrogen in the indole R' group, which is a stable bond as demonstrated through extensive cycling of the electrode. The electrodes demonstrated an average 15 fold increase in sensitivity for dopamine based on current density. In addition, tryptophan modified electrodes were highly selective for dopamine over the interfering biomolecule ascorbic acid. Moving forward, an *in vivo* proof of concept for tryptophan modified electrodes is necessary before dopamine detection can occur in clinical applications.

Table of Contents

List of Figures.....	7
List of Tables.....	8
Abbreviations.....	9
Chapter 1: Introduction.....	10
Chapter 2: Materials and Methods.....	21
Chapter 3: Results.....	24
Chapter 4: Discussion.....	37
Chapter 5: Summary.....	50
Chapter 6: Future Directions.....	52
Appendix.....	54
References.....	58

List of Figures

Figure Number	Description
1	Schematic of cylinder electrode (46)
2	Schematic of tyrosinase modified electrode (18)
3	Cyclic voltammogram for DA, DOPAC, AA (21)
4	Schematic for PEDOT:Nafion electrode and selectivity (20)
5	Proposed mechanism for TRP binding (28)
6	Proposed mechanism for TRP oxidation (30)
7	Pictorial table for TRP derivative compounds
8	Reaction mechanism for TRP derivative compounds
9	Cyclic voltammograms for 0B, 1B, 2A, 2B, 3A, 3B
10	Cyclic voltammogram for 3C
11	Cyclic voltammograms for 1A
12	Nernstian diffusion response plot for 1A
13	Nernstian diffusion response plot for 1 mM TRP
14	Nernstian diffusion response plot for 10 mM TRP
15	Tafel plot for 1 mM TRP
16	Ratio of surface concentration DA, bare and TRP-modified electrodes
17	Sensitivity and durability test for TRP and 1A plating procedures
18	Calibration curve for DA with bare and TRP-modified electrodes
19	Selectivity for DA/AA with bare and TRP-modified electrodes
20	Cyclic voltammograms for DA, AA, with bare and TRP-modified electrodes
21	Proposed scheme for TRP electrode modification
22	TRP chain in DNA photolyase protein structure
Appendix 1	Cyclic voltammogram for TRP
Appendix 2	Cyclic voltammogram for 1 mM and 10 mM TRP, scan rate = 2 V/s
Appendix 3	Schematic for TRP-modified electrode surface area calculation
Appendix 4	Negative control for DA sensitivity
Appendix 5	Negative control for AA sensitivity
Appendix 6	Negative control for ratio DA surface concentration, bare and TRP-modified electrodes
Appendix 7	DA to DQ reaction scheme

List of Tables

Table Number	Description
1	p-values for Fig. 16, surface concentration test
2	p-values for Fig. 17, durability and sensitivity test
Appendix 1	p-values for appendix Fig. 4, negative control for DA sensitivity
Appendix 2	p-values for appendix Fig. 5, negative control for AA sensitivity
Appendix 3	p-values for appendix Fig. 6, negative control for ratio of DA surface concentration

Abbreviations

Abbreviation	Definition
FSCV	Fast-Scan Cyclic Voltammetry
DA	Dopamine
DQ	Dopamine-o-quinone
FSCAV	Fast Scan Adsorptive Voltammetry
TRP	Tryptophan
aCSF	Artificial cerebral spinal fluid
CSF	Cerebral Spinal Fluid
V	Volts
nA	nano amps
PBS	Phosphate buffer saline
UA	Uric acid
AA	Ascorbic Acid
AD	Alzheimer's disease
PD	Parkinson's disease
L-DOPA	Levodopa
PEDOT	poly(3,4-ethylenedioxythiophene)
DOPAC	3,4-dihydroxyphenylacetic acid
5-HTP	5-hydroxytryptophan
XPS	X-ray photoelectron spectroscopy
C-N	Carbon – Nitrogen bond
DOPAC	dihydroxyphenylacetic acid
VMD	Visual Molecular Dynamics

Chapter One: Introduction

Dopamine Background

Dopamine (DA) is a catecholamine neurotransmitter responsible for signal transduction in the neuronal pathways. Dopaminergic neurons are localized in the substantia nigra and ventral tegmental area, releasing dopamine into the caudate nucleus and putamen (1,2). Physiological changes to dopaminergic neurons are associated with cocaine addiction, and neurological disorders, including Alzheimer's disease (AD) and Parkinson's disease (PD).

Degeneration of dopaminergic neurons is prevalent in patients with AD and PD. AD is characterized by the formation of β -amyloid plaques and neurofibrillary tangles (3). PD is characterized by the presence of lewy bodies mainly in the substantia nigra (4). Patients with AD experience loss of memory, whereas patients with PD primarily display bradykinesia (2, 3). The role of DA in AD and PD is not fully understood, however, both are associated with decreased extracellular DA (5). Therapeutic effects have been observed when increased levels of DA are present in AD patients, and the first-line treatment for PD is the dopamine precursor, L-DOPA (6). The role of DA in therapeutic effect and treatment is not fully understood for either disease.

For this project, I sought out to improve the sensitivity of FSCV, an electrochemical analytical tool, for DA detection. Outlined in this thesis is the mechanism of modifying carbon fiber microelectrodes with tryptophan (TRP) and their effect on FSCV to detect DA. This thesis introduces an *in vitro* proof of concept study for tryptophan-modified electrodes with increased sensitivity of DA detection. TRP-modified electrodes with increased sensitivity to DA may help in detecting low levels of DA in PD and AD patients, and may help us understand how different treatments or genes alter the levels of DA in the patient.

Function and Benefits of FSCV

FSCV is an analytical tool used to monitor real time *in vivo* levels of dopamine in the brain (7). A voltage is applied in a triangular waveform, promoting the repeated oxidation of DA to dopamine-o-quinone (DQ), followed by the reduction of DQ to DA. Using carbon fiber microelectrodes, we can quantify the current produced by the cyclic reaction and create a standard curve to further quantify *in vivo* concentrations of DA.

FSCV is not the only tool utilized for analysis of DA levels *in vivo*. Micro dialysis is used to collect and quantify extracellular DA. Micro dialysis requires extraction of cerebral spinal fluid (CSF) to quantify DA levels. Extractions of CSF occur on a minute time scale, making this tool inefficient for monitoring real time changes in DA levels, which occur on a sub-second time scale (7). FSCV outperforms micro dialysis in temporal resolution. For FSCV measurements of DA, we use carbon fiber microelectrodes sealed in glass capillary tubes (8). Microelectrodes possess unique advantages that make them ideal for neurotransmitter detection, the first being their size. Microelectrodes are classified as such when at least one of their dimensions is smaller than 25 μM (9). Their small size reduces the disruption of neuron physiology, limiting the tissue damage during implantation (10). Due to their small area, the double layer capacitance is reduced. Diffusional flux is increased, eliminating the need for stirring to promote mass transport (9). This, in combination with the fast scan rate (generally $> 400 \text{ V/s}$), allows for detection of fast kinetic events, such as DA release.

For DA measurements, cylindrical carbon fiber microelectrodes are utilized (Fig. 1). Scanning was performed at a frequency of 10 Hz. The triangular wave form applied has a resting potential of -0.4 V in between triangle waveforms, and a potential window of $-0.4 - 1.3 \text{ V}$ (vs. Ag/AgCl). In physiological conditions, DA is positively charged. Pretreatment of the electrode

via cycling in supporting electrolyte promotes oxidation of the carbon surface. Thus, during the holding potential between applied cycles, DA is adsorbed

onto the surface of the electrode. However, there is a tradeoff for this phenomenon; if the frequency is reduced to the time frame for DA to adsorb to the surface and increase its sensitivity, temporal resolution can be lost. Fast Scan Cyclic Adsorptive Voltammetry (FSCAV)

utilizes a waveform to address this issue (11). For this study, the traditional triangular waveform was applied at a frequency of 10 Hz. The temporal resolution of

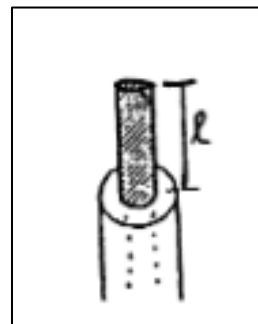


Fig 1. Schematic of a cylinder microelectrode. The gray region represents the carbon fiber, white representing the glass capillary tube the carbon fiber is enclosed within (46).

traditional FSCV is still superior to micro dialysis, with sampling occurring on the millisecond time scale as opposed to minutes (12).

Performance of Modified Electrodes

Multiple approaches have been utilized to increase FSCV detection for DA, including waveform manipulation and boron doped diamond electrodes (BDD) (13,14). Waveform manipulation relies on changing the waveform of the applied potential, which can lead to reduced noise and in some cases, change surface chemistry of the redox reaction. On the other hand, BDD were shown to have increased stability for long term implantation in human subjects (14). These approaches involve modification of the entire electrode or the parameters of FSCV, which are different from my project that aims to modify the electrode surface by means of deposition of an organic molecule. Modification of the electrode surface has been practiced in previous studies, a few of which are outlined in this thesis.

Biochemical sensors have used immobilized tyrosinase, an enzyme which promotes oxidation of phenol groups, to electrochemically detect phenolic compounds (15). *In situ*,

tyrosinase is responsible for oxidation of precursors in the DA metabolic pathway (16). This understanding led to the development of tyrosinase based electrodes for FSCV detection of DA, a phenolic-like catecholamine (17,18).

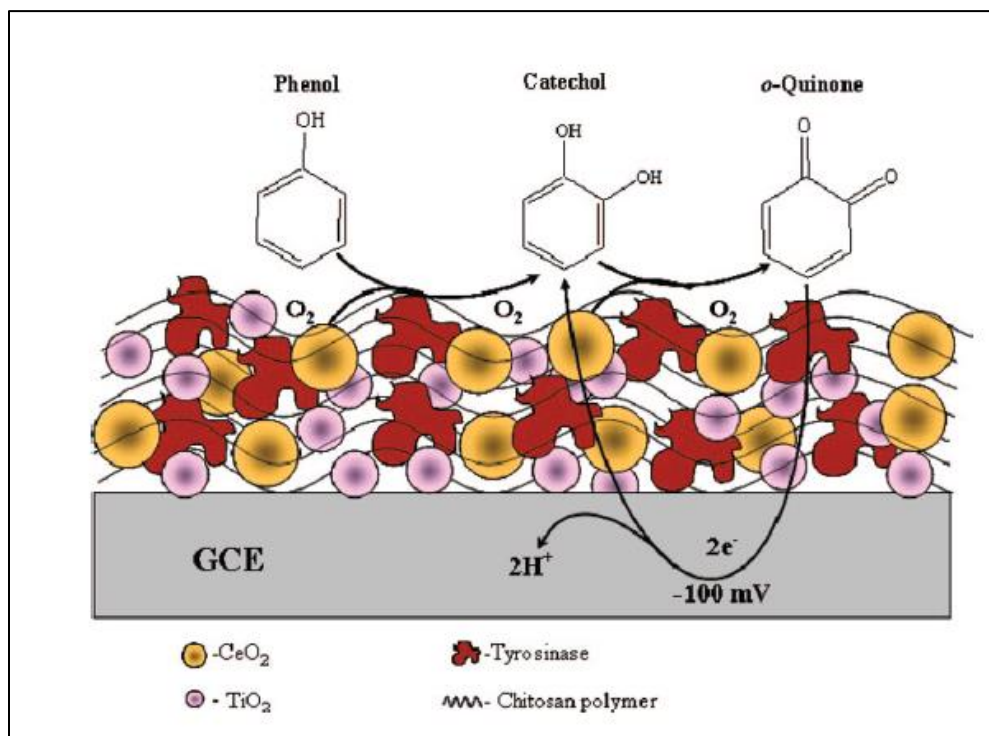


Fig. 2. Schematic of the tyrosinase modified electrode. Tyrosinase enzyme, CeO_2 and TiO_2 are embedded in the chitosan polymer, promoting oxidation of DA (18).

Electrodes modified with tyrosinase were done by using a four component system. The first component was the chitosan matrix, a nontoxic glucosamine polymer capable of crossing the blood brain barrier (19). Immobilized in the chitosan matrix were the second component, tyrosinase enzymes and the final two components, two different metal oxides, CeO_2 and TiO_2 . The four components of the surface modification are illustrated in Fig 2. with the reaction scheme for oxidation of phenol depicted above the modified surface. Tyrosinase, when in the presence of CeO_2 and TiO_2 , can catalyze the oxidation of DA, similar to the oxidation process for a phenol group. The oxidation – reduction reaction from DA is shown in Appendix Fig 7.

The observed increased sensitivity of FSCV for DA was attributed to faster kinetics of oxidation (18). Prolonged measurement of DA indicated a stable increase in sensitivity for DA for 100 minutes before dropping off. Selectivity was investigated using chronoamperometry. Ratio of DA current/interfering molecule current was used to calculate the increase in response to DA over the interfering molecule. DA/L-DOPA was 178.62 ± 10.67 and 5.12 ± 0.60 for DA/3,4-dihydroxyphenylacetic acid (DOPAC); no amperometric response for uric acid (UA) or ascorbic acid (AA) was observed. Control sensitivity for DA was 1.7 ± 0.05 nA/ μ M, while the modified electrode was drastically improved with 14.2 ± 0.50 nA/ μ M.

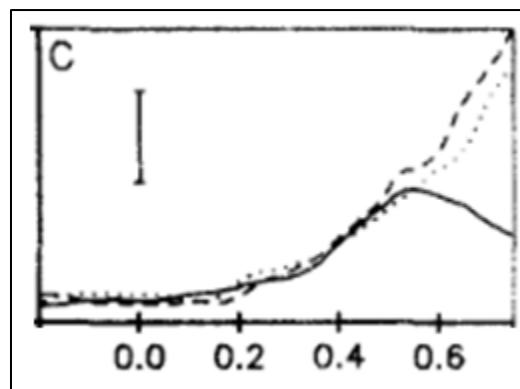


Fig. 3. Cyclic voltammograms for detection of DA (solid line), DOPAC (dashed line), and AA (dotted line) at a scan rate of 300 V/s. Current bar is 3 nA (21).

Non-enzymatic, multi-component surface modifications have also been shown to increase FSCV sensitivity for DA. For example, Nafion is a copolymer of polytetrafluoroethylene with per fluorovinyl ether sulfonic acid side chains (20). Previous work has shown that nafion-modified electrodes improve selectivity for DA over interfering electroactive chemicals. Fast-scanning at 300 V/s with DOPAC and ascorbate resulted in indistinguishable oxidative potentials, as shown in Fig.3 (21). Improved selectivity using nafion was thus characterized by the ratio of current measured for DA to interfering molecule. DA/ascorbate current ratio reported was 1300 ± 280 , and 480 ± 190 for DA/DOPAC. This improved selectivity for DA is attributable to nafion's negative charge at physiological pH (20). Whereas DA is positively charged and attracted to the nafion coated surface, interfering molecules such as ascorbate and DOPAC are

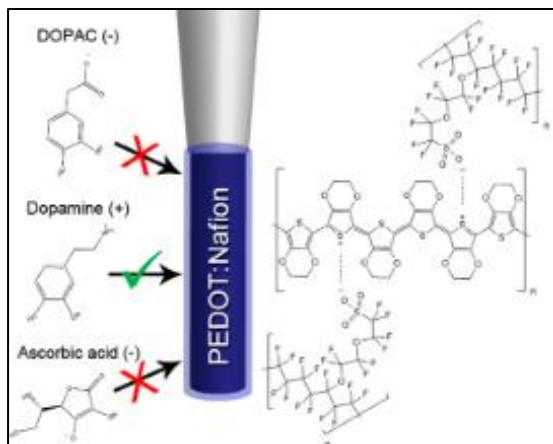


Fig. 4. Selectivity mechanism for PEDOT:Nafion coated electrode. Negatively charged DOPAC and AA are repelled by the negatively charged surface. Conversely, positively charged DA is attracted to the surface (20).

repelled due to their negative charge at physiological pH (20).

Vreeland et al. (2015), developed a two component electrode surface modification with nafion and poly(3,4-ethylenedioxythiophene) (PEDOT). Polymerization of PEDOT produces a

positive charge on the surface, which is in turn

balanced by the negative charge of the nafion (22).

DA/AA selectivity ratio reported for PEDOT:nafion

coated electrodes was 1540 ± 150 , and 52 ± 4 for DA/DOPAC. High density PEDOT: nafion (400 μM) coating had a 4-fold increase in sensitivity, from 13 ± 2 nA/ μM for the bare electrode, to 46 ± 13 nA/ μM for the coated electrode. A schematic of the PEDOT:nafion selectivity mechanism is depicted in Fig 4. The two component surface modification (PEDOT, nafion) yielded increased sensitivity and selectivity for FSCV measurements of DA. However, the mechanism behind the increased sensitivity is not understood (20).

Tryptophan Modified Electrodes

Tryptophan (TRP) is an aromatic amino acid often conserved in homologous protein sequences. Therefore, the function of tryptophan in catalytic enzyme chemistry has been of interest. Analysis of the Enzyme Data Bank of the Swiss Institute of Bioinformatics revealed that frequency of TRP residues in oxoreductases is above the total average TRP frequency in the entire data bank (23). Electron transfer can occur over distances of 10-15 Å in proteins (24). The aromatic rings in TRP assist in this transfer by serving as a hopping point for electrons to pass through. One example of this is in cytochrome C, where TRP was found to be conserved, and

responsible for catalysis of oxidative enzymatic function (25,26). Therefore, it was hypothesized that TRP can increase the rate of oxidation and reduction in other electrochemical processes, such as DA to DQ, in cyclic voltammetry.

Lin and Li 2006, investigated this hypothesis using TRP-modified electrodes for cyclic voltammetry detection of DA (27). Electrode modification was performed using cyclic voltammetry in a potential window of -1.7 to 1.8 V, and a scan rate of 0.02 V/s. Cyclic voltammograms revealed an irreversible oxidation of TRP on the surface, resulting in a monolayer coating (28). Electrodes were modified with either TRP or 5-hydroxytryptophan (5-HTP) initially for UA and AA. 5-HTP electrodes outperformed TRP electrodes in UA and AA detection. Simultaneous detection of UA and AA was possible for modified electrodes, which were scanning at 0.05 V/s (difference in E_p). Sensitivity tests revealed TRP-modified electrodes were the least sensitive of the modified electrodes for UA and AA. Lin and Li 2009 investigated 5-HTP and TRP-modified electrodes for increased DA sensitivity. Again, 5-HTP-modified electrodes outperformed TRP-modified electrodes with average increases in DA sensitivity of 12.4 and 7.8, respectively.

These electrodes were all used at slow scan rates < 0.1 V/s for the detection of DA, UA, and AA. For my project, I have investigated TRP-modified electrodes for their increased sensitivity for DA, selectivity for DA over interfering molecules, and durability of the coating. Despite the 5-HTP-modified electrodes being more sensitive than TRP electrodes for DA, 5-HTP electrodes were not considered for my research. AA sensitivity for 5-HTP –modified electrodes was 2.9 times greater than for a bare electrode whereas TRP-modified electrode sensitivity for AA was 0.9 times that of a bare electrode. The tradeoff for loss of sensitivity using TRP over 5-HTP is outweighed by the decreased response for the interfering molecule AA. At slow scan

rates, AA could be differentiated from DA due to different oxidative E_p (21). This difference is not observed at fast scan rates, therefore, differences in peak oxidation current must be used to quantify selectivity. Thus the decrease in peak current oxidation for TRP electrode, compared to 5-HTP is a benefit.

Besides selectivity, the mechanism of TRP deposition was investigated for further optimization of the deposition procedure. Nernstian diffusion responses were assessed, as well as concentration and scan rate dependency. Durability of the modified surface was evaluated by evaluating DA sensitivity after deposition, and after the electrode was exposed to extensive cycling, to show stability of the modified surface over time.

Tryptophan Reaction Mechanism

The mechanism by which TRP modifies to the surface of the carbon electrode is not fully understood. Consistent reports indicate that TRP undergoes an irreversible oxidation reaction with the carbon surface (28,29). The Lin and Li 2006 paper proposed a reaction mechanism for 5-HTP as seen in Fig 5. Since TRP does not contain the 5' hydroxyl group, the proposed mechanism for TRP could then be a one electron oxidation at the amine group, generating the reaction nitrogen which can covalently bond with the carbon surface. However, Baytak et al. (2015) proposed that there was a two electron oxidation occurring. The Lin and Li 2006 paper confirmed that 5-HTP had a carbon – nitrogen (C – N) bond via X-ray photoelectron spectroscopy (XPS). Baytak et al. (2015) used a Tafel plot to experimentally derive the number of electrons in the oxidation of TRP. Fig. 6 shows the reaction scheme for TRP oxidation proposed by Baytak et al. (2015). Focusing on the Lin and Li 2006 XPS results, we can infer that TRP is also forming a C – N bond with the carbon surface. The nitrogen's in 5-HTP are located at the same positions in TRP. However, which nitrogen is participating in the C – N bond, the

amine nitrogen of the backbone or the nitrogen in the R side group (indole), is unknown. Baytak et al. (2015) had a different potential window for TRP cyclic voltammetry, 0.2-0.9 V. Additionally; they were using a multi-walled carbon nanotube electrode modified with nanoparticles of nickel. Lin and Li used LiClO_4 , an oxidizing agent, whereas Baytak et al. did not. This may have oxidized tryptophan before deposition, changing the number of electrons in the oxidation caused during voltammetric deposition. Therefore, it is not clear how many electrons were lost, or at what nitrogen position it occurs at, which leads to the molecules irreversible oxidation and subsequent covalent bonding to the carbon electrode surface.

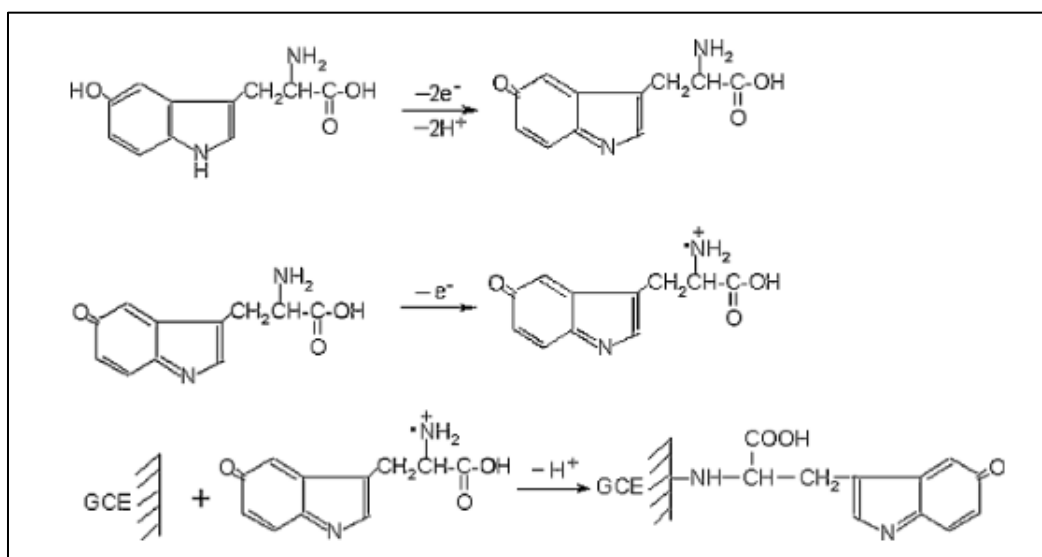


Fig. 5. Proposed mechanism for irreversible oxidation of 5-HTP on a glassy carbon electrode. Here, the carbon – nitrogen bond is hypothesized to use the nitrogen in the amine of the amino acid backbone (28).

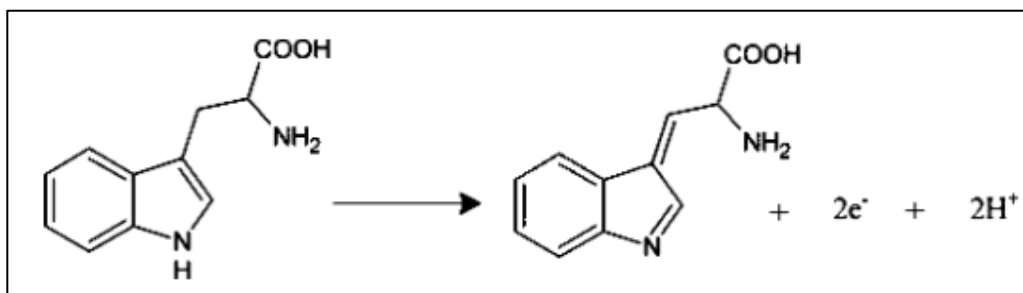


Fig. 6. Proposed mechanism for irreversible oxidation of TRP on a multi-walled carbon nanotube electrode modified with nanoparticles of nickel. Here, the carbon – nitrogen bond is hypothesized to use the nitrogen of the R chain of the amino acid (30).

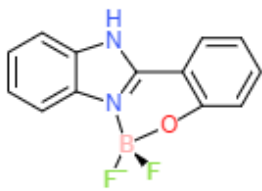
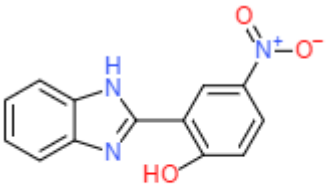
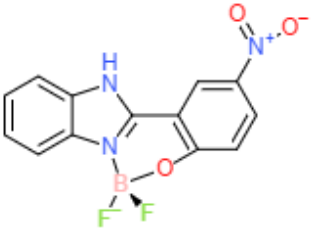
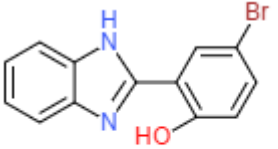
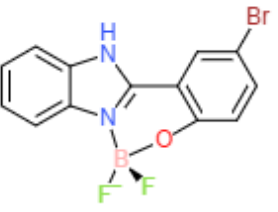
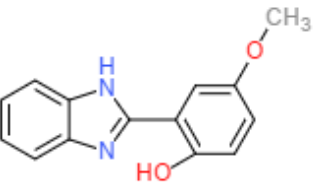
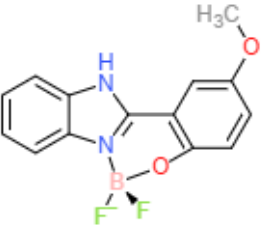
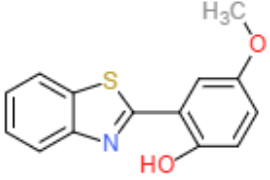
Free Ligand	Boron Complex
	 0B
 1A	 1B
 2A	 2B
 3A	 3B
<p>*</p>  3C	

Fig. 7. Naming scheme for the tryptophan derivatives. Number depicts 5' R group substitution. *Compound 3C contains a thiozole.

Tryptophan Derivatives

In addition to TRP, eight TRP derivatives synthesized in the Korich lab (Grand Valley State University) were assessed for potential electrode modification and increased sensitivity for DA (Fig 7). The benzimidazole compounds complexed with boron were synthesized from 2-(2'-hydroxyphenyl) benzimidazole and boron trifluoride etherate in methylene chloride. A reaction scheme for compound synthesis is displayed in Fig 8. These compounds are derivatives of tryptophan, containing the same structure as the R group. In place of the peptide backbone however is a phenyl group, with different substitutions at the 5' position. Based on the similar R chain as tryptophan, we hypothesized that these compounds might also confer increased DA electron transfer kinetics due to "electron hopping" observed in tryptophan in experimental compounds.

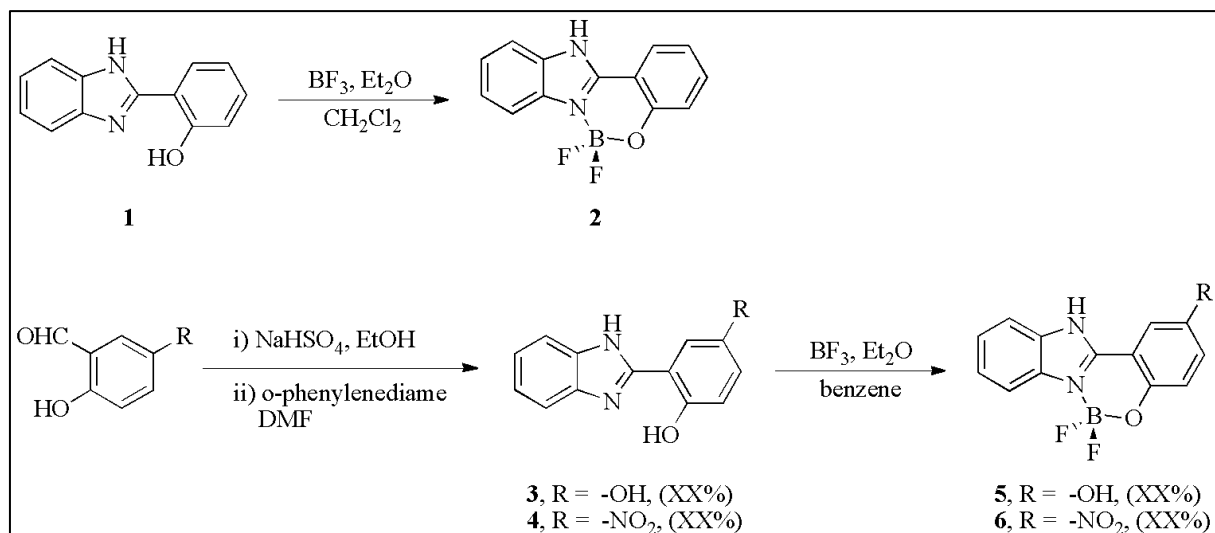


Fig. 8. Reaction mechanism for the tryptophan derivatives synthesized in the Korich lab

Chapter Two: Materials and Methods

Solutions

Artificial Cerebral Spinal Fluid (aCSF) used in all DA collections was made with 125 mM NaCl, 4 mM KCl, 1.3 mM CaCl₂, 1 mM MgCl₂, 0.66 mM NaH₂PO₄, 2 mM Na₂HPO₄, 1 mM glucose; pH 7.4 (30). Experimental compounds were made in 100 % DMSO. PBS used contained 140 mM NaCl, 3 mM KCL, 10 mM NaH₂PO₄; pH 7.4 (31). Tryptophan derivative solutions were made with 1 mM compound. TRP deposition was performed with 1 and 10 mM TRP, and 10 mM LiClO₄ (28). 200 μ M AA were used for selectivity tests (17).

Electrode Preparation

Cylindrical microelectrodes were made using 7 μ M diameter carbon fiber, cut to an average length of 100 μ M, and sealed in a glass capillary tube with paraffin (8). Electrodes were cycled in aCSF for 15 minutes at 60 Hz, then for 5 minutes at 10 Hz, in a potential window of -0.4 to 1.0 V. This cleaned the electrode surface and generated oxide layer (32). Electrode length was measured with an AmScope stereoscope and ToupView software. All experiments were performed vs. an Ag/AgCl reference.

Tryptophan Deposition

Experiments with scan rates ≤ 2 V/s were performed using a 1200B model CH Instruments potentiostat and its accompanying software. Experiments with scan rates > 2 V/s were performed using a Dagan chemclamp potentiostat and analyzed with DEMON software. Electrodes modified at scan rates ≤ 2 V/s ran for 3 complete cycles (6 segments). Electrodes modified with DEMON were modified using the working electrode as a stimulating electrode, and a transistor. The transistor comprised of 2 led lights which allowed control over the start of

the experiment by delaying the start of stimulation. Therefore the application of the potential to the working electrode was applied after a 5 second delay, allowing for collection of data at the start of the experiment. DEMON settings for deposition were: Frequency: 1 Hz; Amp: 3 V; Polarity Monophasic: +; Delay: 14 ms; Offset: 0; Pulse Width: 999 ms; Paired Pulse: Single. Stimulation time delay was 5 seconds. For the experiments > 2 V/s, (20 V/s and 200 V/s), collections with DEMON were performed for 20 seconds with a 5 second STIM start delay, 10 pulses, and a 5 second off period before ending.

Sensitivity and Durability

Bare electrodes used for sensitivity and durability tests were cycled in aCSF for 15 minutes at 60 Hz, then 5 minutes at 10 Hz, in a potential window of -0.4 to 1.0 V. All DA collections were performed for 30 seconds with concentrations of DA at 50 nM, 100 nM, 200 nM, 500 nM, or 1 μ M. In between each collection, the electrode was allowed to briefly cycle in aCSF to remove DA still on the carbon surface. Before deposition, electrodes were cycled in PBS for 10 minutes at 10 Hz in a potential window from -.4 to 1.0 V to clean the surface. Extended cycling of electrodes was done in aCSF for 10 minutes at 60 Hz and 5 minutes at 10 Hz.

Extended time collections for durability were performed for 2 hours. DEMON settings for the 2 hour collection were: Collection Duration – 60 seconds, Number of files – 120, Collection Interval – 0. Background subtraction was performed using Octave.

Selectivity

Electrodes used for selectivity tests were cycled in aCSF for 15 minutes at 60 Hz, then 5 minutes at 10 Hz, in a potential window of -0.4 to 1.0 V. FSCV was used to measure 200 μ M

AA and 1 μ M DA independently with the bare electrode, and after extended cycling of the TRP-modified electrode. Collections were performed for 30 seconds, Frequency: 10 Hz, potential window: -0.4 – 1.0 V. 1 mM TRP was used to modify electrodes, scan rate = 0.02 V/s, potential window: -1.7 – 1.8 V. Ratio of current density for DA/AA was used for analysis.

Statistical Analysis

All statistical analyses were performed using R. Pairwise *t* tests and ANOVA were performed for all comparative analyses.

Chapter Three: Results

Electro Reactivity of Experimental Compounds

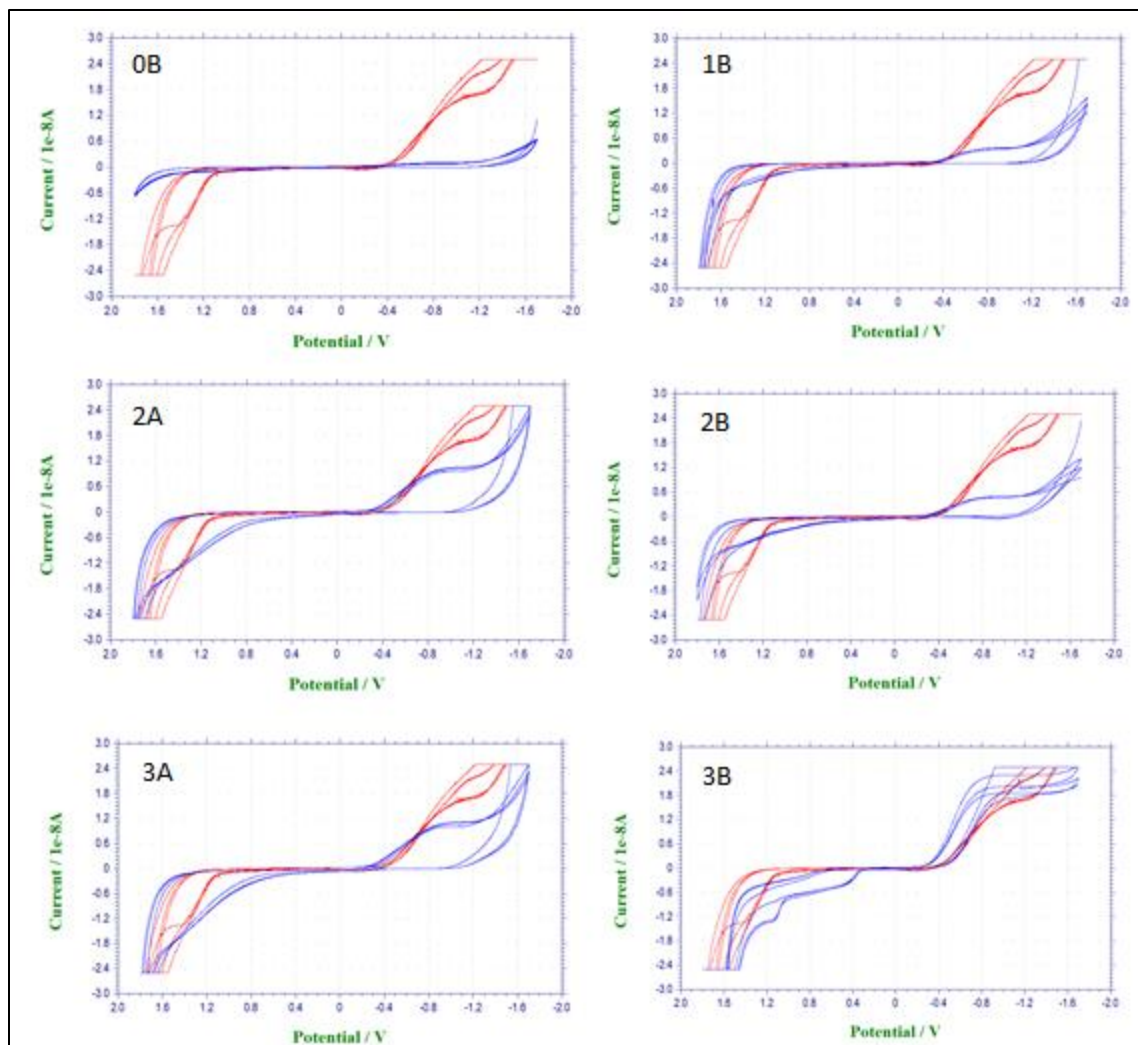


Fig 9. Cyclic voltammograms for compounds 0B, 1B, 2A, 3A, and 3B. Negative control is displayed in red, experimental compound in blue. All experiments were performed with 1 mM compound, -1.7 – 1.8 V, scan rate = 0.02 V/s.

The 8 experimental compounds were first tested for oxidation/reduction reactions using cycling voltammetry in a potential window of -1.7 to 1.8 V and a scan rate of 0.02 V/s. Six of the eight compounds; 0B, 1B, 2A, 2B, 3A (Fig. 9), did not show an oxidation or peak in the first sweep, implying that they were not electro reactive. Compound 3B showed an oxidation peak

with no subsequent reduction peak, however, this peak was still present in successive sweeps. If there is a peak present in the first sweep, but not successive sweeps, it is indicative of a monolayer reaction. The oxidation peak decreases due to saturation of the surface with the compound. If the oxidation peak grows after successive sweeps, it is indicative of a growing polymer on the surface. The oxidation peak for 3B did not increase or decrease in peak current after successive sweeps, therefore, there was no evidence indicating the compound was interacting with the surface of the electrode. Therefore, these compounds were not investigated further. Compound 3C (Fig. 10), was tested using an injection method, where the compound was added to the solution after the first 3 cycles had passed. The cyclic voltammogram for compound 3C did not indicate an irreversible reaction. There were no distinct oxidation or reduction peaks, therefore, presence of a reversible or irreversible reaction could not be determined. Compound 1A had an oxidation reaction occur in the first cycle, but not in the successive cycles (Fig. 11b). This result was similar to that of an irreversible reaction at the electrode surface, and has been seen in cyclic voltammograms for TRP. (28,33,34). In the first cycle, sweeping from -1.7 to 1.8 V showed a distinct oxidation peak, however, the reverse sweep from 1.8 to -1.7 V did not show a reduction peak. This implies that the compound was irreversibly oxidized. As well, the oxidation peak decreased in size during successive cycles, suggesting the compound may be saturating the surface of the electrode, and therefore is binding to the surface of the electrode. Compound 1A was also tested in a potential window was adjusted to -0.4 to 1.3 V to eliminate water reactions which might degrade the carbon surface. Adjusting the potential window increased the peak oxidation current (Fig. 11a). This potential window was used for further investigation of compound 1A at the surface of the electrode.

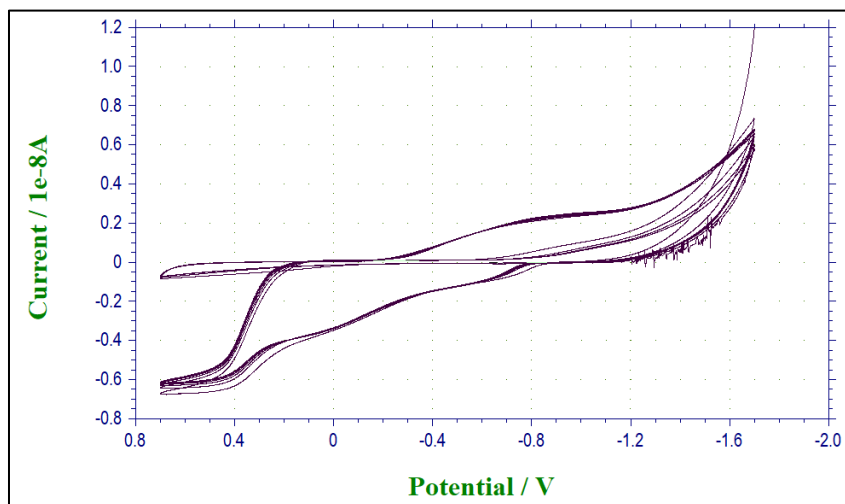


Fig 10. Cyclic voltammogram for compound 3C. After the first 3 complete cycles, compound 3C was injected. 1 mM 3C was used in a window of -1.7 – 1.8 V, scan rate = 0.02 V/s.

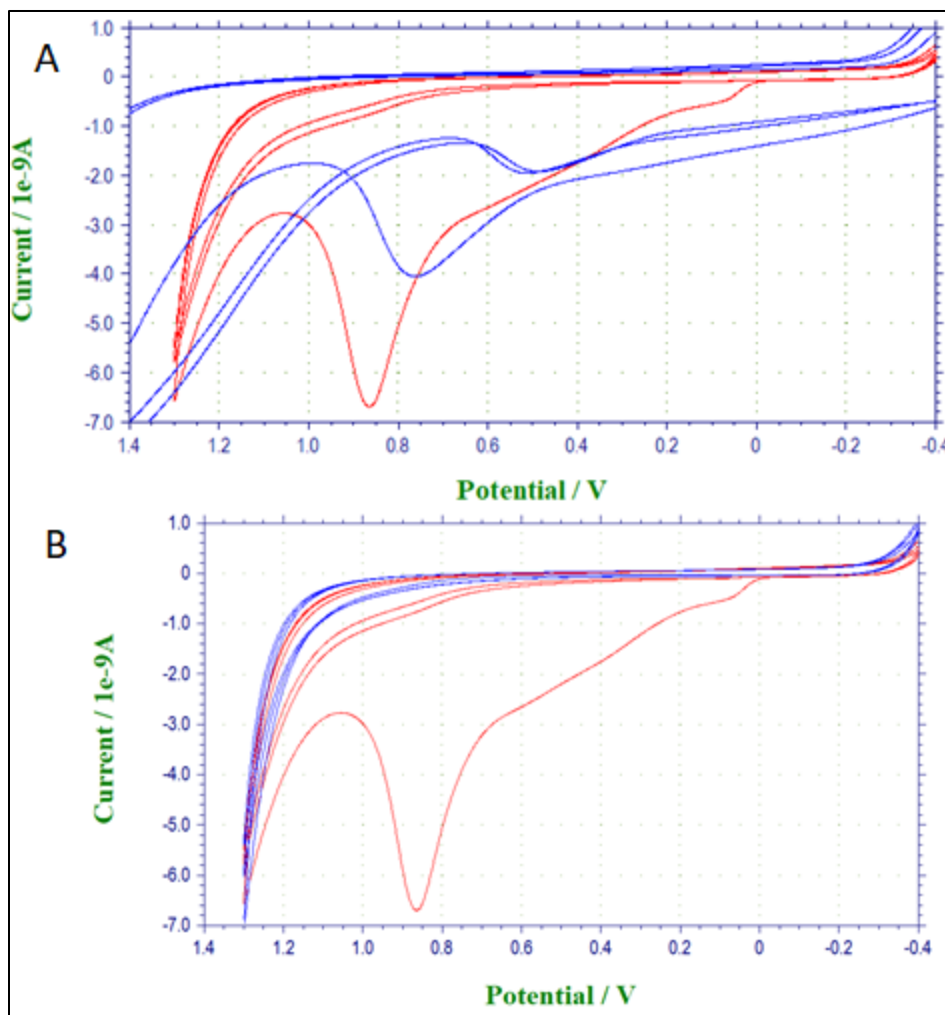


Fig 11. A.) 1 mM 1A, potential window -1.7 – 1.8 V (blue), -0.4 – 1.3 V (red). Scan rate = 0.02 V/s. B.) 1 mM 1A (red), negative control (blue), potential window -0.4 – 1.3 V. Scan rate = 0.02 V/s.

Nernstian Diffusion Response

To test if Compound 1A's irreversible reaction was diffusion controlled, a logarithmic transformation of the scan rate and peak current density was plotted (Fig 12). If the slope of the linear regression line is 0.5, the reaction is diffusion controlled; and when it is 1, it is adsorption controlled. For 1A, the logarithmic transformation of the scan rate vs. peak current density was fit with a linear regression line, with a slope of 0.466, indicative of a diffusion controlled process. Diffusion behavior at cylindrical microelectrode is similar to planar diffusion at fast scan rate when the radius of the microelectrode is sufficiently small and the electrode is

sufficiently long (35). Therefore, scan rates ≥ 0.2 V/s were used in order to use the following relationship for planar electrodes to describe the cylindrical microelectrodes.

$$i_p = (2.69 \times 10^5) n^{3/2} A D_o^{1/2} C_o^* v^{1/2} \quad (1)$$

Equation (1) is the peak current for a diffusing species; i_p : peak current (A); n : number of electrons; A : surface area (cm^2); v : scan rate (V/s); D_o : diffusion coefficient (cm^2/s), C_o^* : bulk concentration (mol/cm^3). For TRP, the slope of the linear regression line was 0.5042, indicating a diffusion controlled reaction (Fig. 13). The slope for 10 mM TRP was 0.4667 (Fig 14).

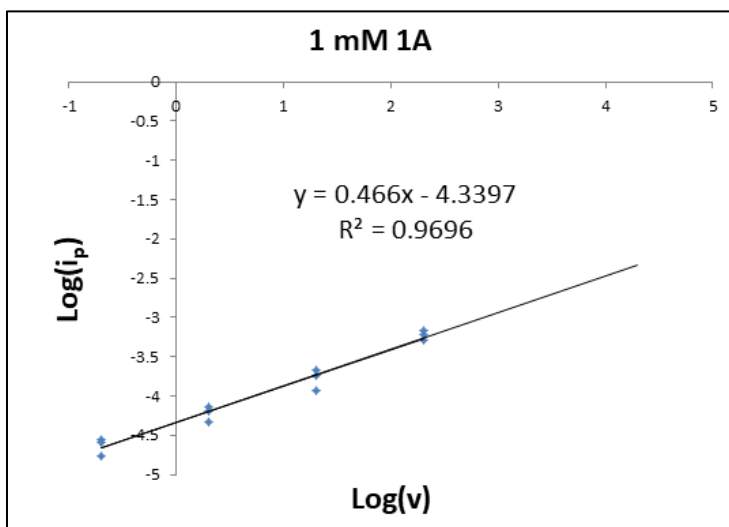


Fig 12. Log transformation of scan rate vs. current density for the oxidation of 1A. The coefficient for the slope of the line 0.466

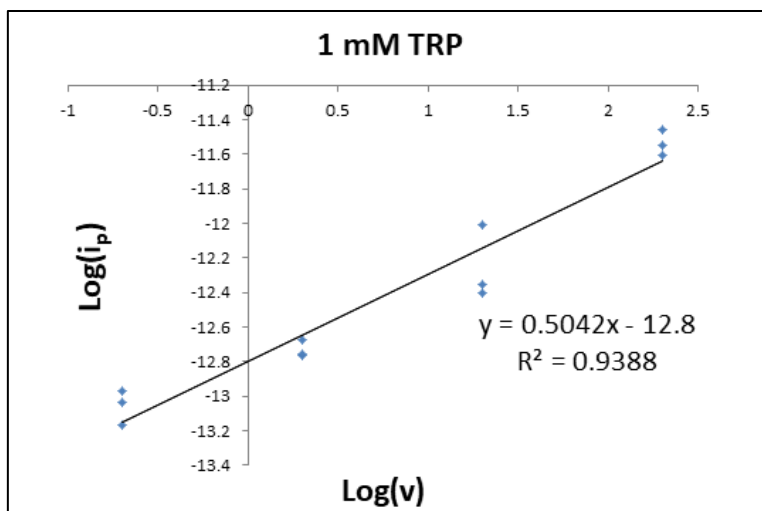


Fig 13. Log transformation of scan rate vs. current density for the oxidation of 1 mM TRP. The coefficient for the slope of the line was 0.5042.

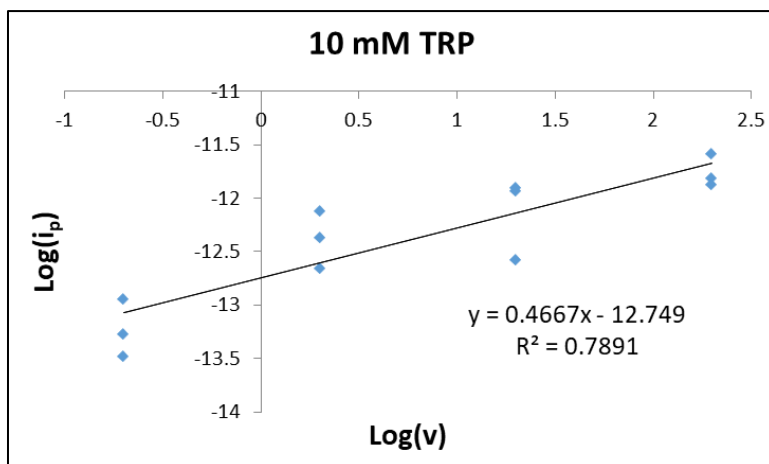


Fig 14. Log transformation of scan rate vs. current density for the oxidation of 10 mM TRP. The coefficient for the slope of the line was 0.4667.

Tafel Plot

A Tafel plot for the E_p vs. $\ln(v)$ was made for scan rates of 0.02 , 0.2, 2, 20, and 200 V/s using 1 mM TRP based on the following equation:

$$E_p = E^0 + \frac{(RT)}{(anF)} + \frac{\ln(RTK^0)}{(anF)} + \frac{(RT)}{(anF)} \ln v \quad (2)$$

E_p : Potential of oxidation peak (V); E^0 : formal potential; R: gas constant (8.314 J/mol); T: temperature (K); K^0 : standard rate constant; α : electron transfer coefficient; n: electrons oxidized or reduced; F: Faradays constant (96487 C/mol). The slope of the linear fit line was 0.0522, yielding an n of 0.984, indicating an oxidative loss of one electron (Fig 15). An electron transfer coefficient, α , for an irreversible process of 0.5 was used as an approximation for this calculation (29).

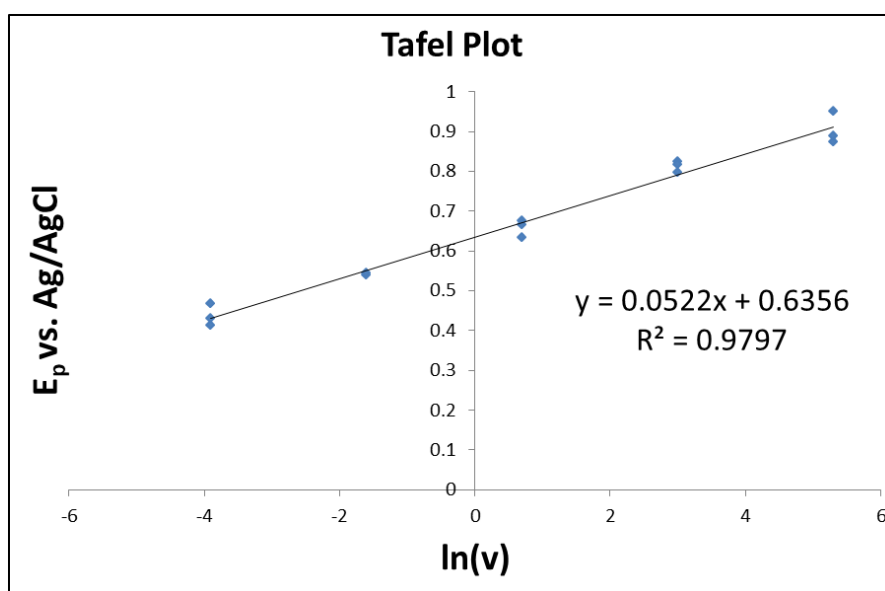


Fig 15. Tafel plot for 1 mM TRP deposited in a window of -1.7 – 1.8 V, scan rates = 0.02, 0.2, 2, 20, & 200 V/s.

Surface Concentration

Approximate surface concentration of DA (mol/cm^2) was calculated for modified and unmodified electrodes (Fig 16.) Integration under the oxidation peak was used to estimate the charge contribution Q .

$$Q = nFA\Gamma \quad (3)$$

Equation (3) was used to solve for the surface concentration of DA, Γ . Q: charge (coulomb); n: electrons transferred; F: Faradays constant (96487 C/mol); A: area (cm^2); Γ : surface concentration (mol/cm^2). Ratio of Γ was calculated Bare/After deposition, and Bare/After Cycling, for 1 mM TRP and 10 mM TRP deposited at 0.02 V/s. P-values are displayed in table 1. Electrodes modified with 1 mM TRP had a significant increase in Γ for collections after deposition, and after extended cycling. Electrodes modified with 10 mM TRP had a significant increase in Γ after extended cycling of the modified electrode. Negative control data for electrodes modified with TRP is shown in Appendix Fig 6 with corresponding p-values shown in table 3. There was no significant difference between electrodes treated with PBS and electrodes treated with PBS and TRP and LiClO_4 (p- value = 0.091), however, there was a general trend for increased surface concentration using electrodes modified with PBS, TRP, and LiClO_4 .

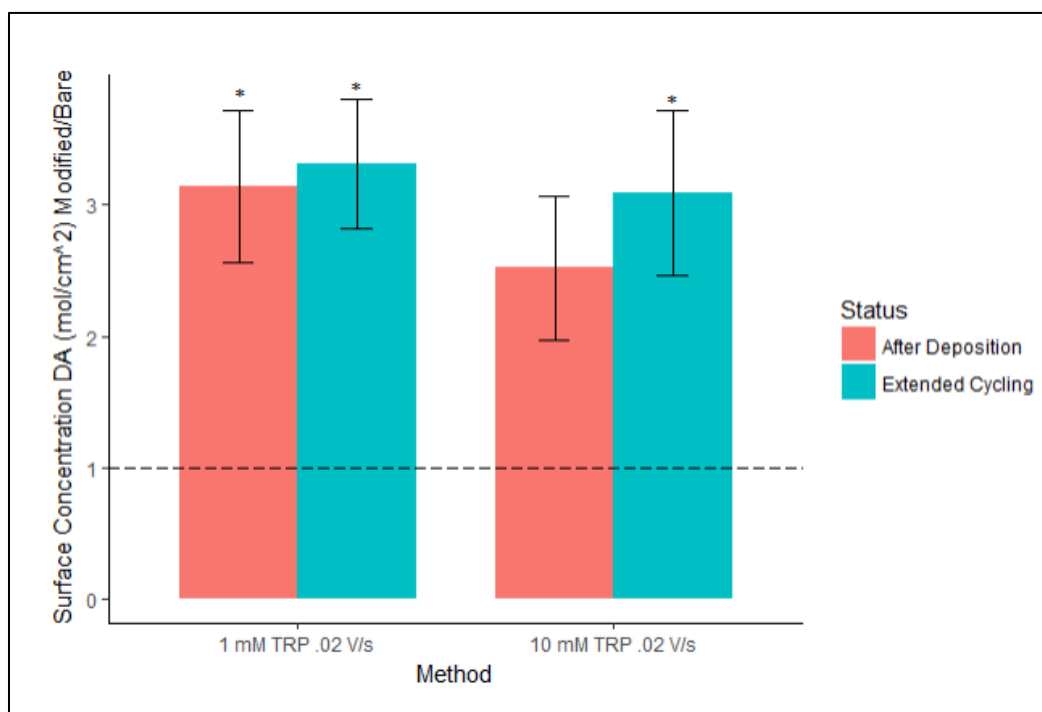


Fig 16. Ratio of surface concentration for DA based on area under the curve of the oxidation peak. After deposition/Bare (red), Extended Cycling (blue). Error bars represent standard error. * indicates a significant difference between experiment and control.

	1 mM TRP	10 mM TRP
After Deposition/Bare	.022*	.16
Extended Cycling/Bare	.014*	.04*

Table 1. p-values associated with tests in Fig 16, $\alpha = 0.05$

Monitoring DA

To determine the most effective deposition method for detection sensitivity, electrodes were modified with 1 mM TRP at 0.02 V/s, 10 mM TRP at 0.02 V/s, 10 mM TRP at 2 V/s, and 1 mM 1A at 0.02 V/s. FSCV was used to measure 1 μ M DA before deposition, immediately after deposition, and after the modified electrodes were allowed to cycle for an extended period, to show repeatability after an extensive amount of potential waveforms were applied to the electrode. Extended cycling was done at 60 Hz for 10 minutes, followed by cycling at 10 Hz for 5 minutes. Results for extended cycling are shown in Fig. 17. Corresponding p-values are displayed in Table 2. Electrodes deposited with TRP at 0.02 V/s had significantly increased sensitivity for DA after deposition. Electrodes modified with TRP at 2 V/s showed no significant increase in sensitivity for DA. There was no significant change in sensitivity for DA after deposition of TRP and after extended cycling of the TRP-modified electrode, when the electrodes were modified with a scan rate of 0.02 V/s. 1A-modified electrodes had a significant decrease in sensitivity for DA immediately after deposition, but not after extended cycling (Fig 17).

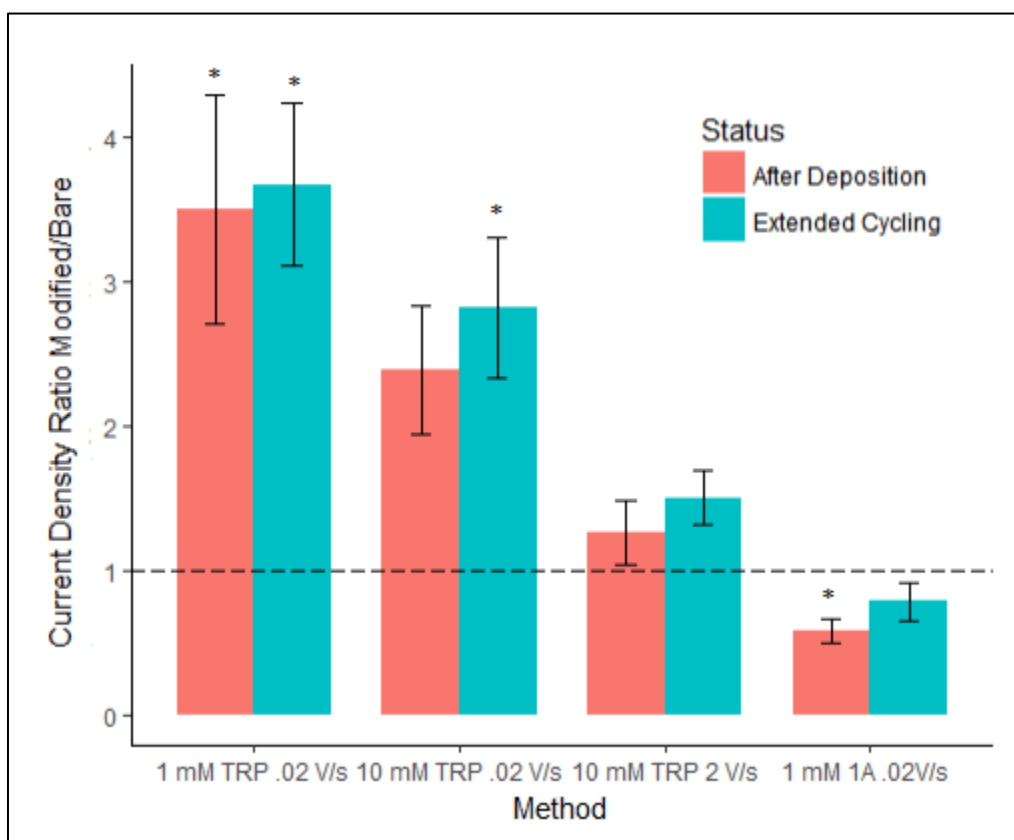


Fig 17. Results for 4 different deposition procedures: 1 mM TRP at 0.02 V/s, 10 mM TRP at 0.02 V/s, 10 mM TRP at 2 V/s, 1 mM 1A at 0.02 V/s. Current density ratio for DA After Deposition/Bare (red) and Extended Cycling/Bare (blue) plotted. Error bars represent standard error. * indicates a significant difference.

	1 mM TRP .02 V/s	10 mM TRP .02 V/s	10 mM TRP 2 V/s	1 mM 1A .02 V/s
After Deposition/Bare	.024*	.028*	.91	.028*
Extended Cycling/Bare	.034*	.092	.19	.366

Table 2. p-values associated with tests in Fig 17, $\alpha = 0.05$.

Extended DA collections were also performed to evaluate durability. DA collections were performed for 20 seconds with the bare electrode prior to TRP deposition. DA collections using modified electrodes were performed for 2 hours. Sensitivity for DA decreased gradually after 8 minutes, and continued to decrease for the remainder of the collection.

Calibration Curve

A calibration curve for a bare electrode and a TRP-modified electrode is shown in Fig 18. Electrodes were modified with 1 mM TRP, and cycled after TRP deposition for 10 minutes at 60 Hz then 5 minutes at 10 Hz. 50, 100, 200, 500, and 1000 nM DA standards were used. The slope for the curve of the bare electrode and the TRP-modified electrodes were $3.974\text{e-}08 \pm 5.358\text{e-}09$, and $7.662\text{e-}08 \pm 5.421\text{e-}09$, respectively. The slope for the TRP-modified electrode curve was 1.93 times greater than that of the bare electrode.

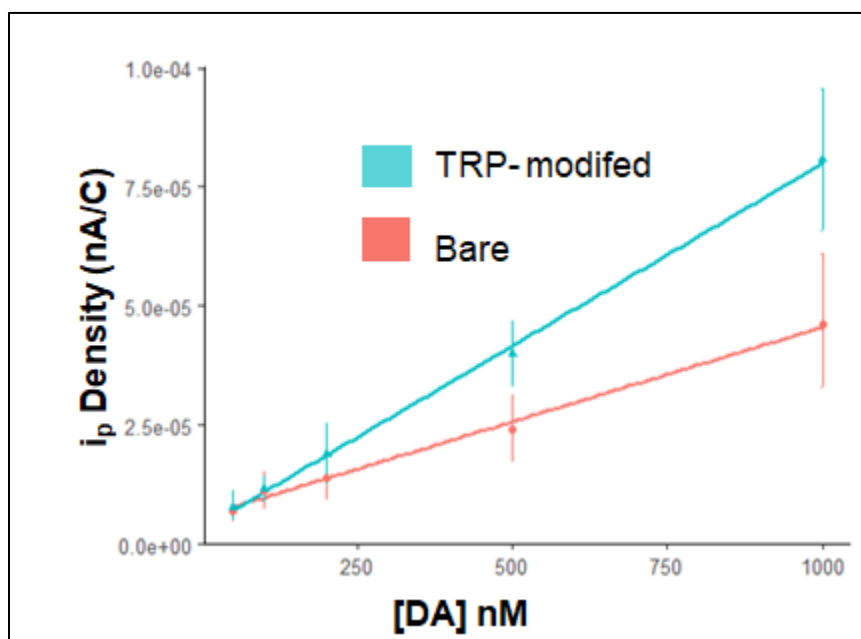


Fig 18. Concentration of DA vs. current density. Integration of background used as an estimate of electrode size for normalization. Error bars represent standard error. Bare electrode (blue), TRP-modified electrode after extended cycling (red).

Selectivity

Independent collections were performed for 1 μM DA and 200 μM AA using a bare electrode and a TRP-modified electrode. Electrodes were modified with 1 mM TRP at 0.02 V/s,

and cycled after TRP deposition for 10 minutes at 60 Hz then 5 minutes at 10 Hz prior to DA and AA collections. Ratio of DA/AA peak oxidation current density was used to evaluate selectivity of electrodes before and after TRP deposition (Fig 19). Student's pairwise t test yielded a p-value of .014* indicating a significant difference in the current density for DA/AA before and after modification. Fig 20. displays cyclic voltammograms for DA and AA independent collections before and TRP deposition, showing DA amperometric response increasing with modification, and AA response decreasing.

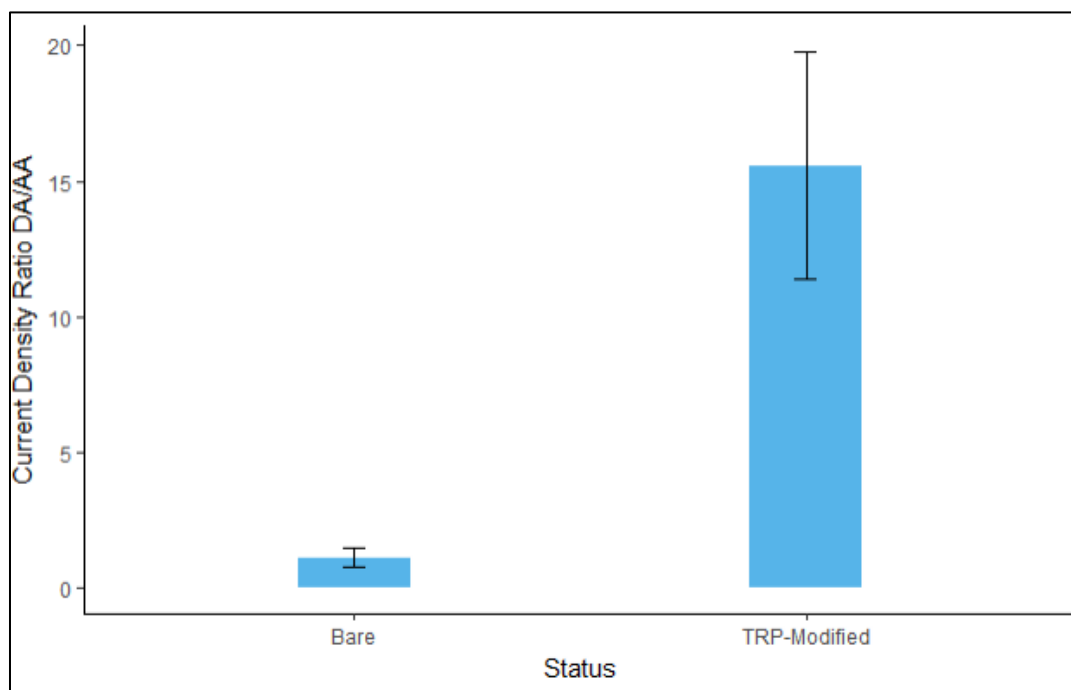


Fig 19. Ratio of current density for independent collections of DA and AA. TRP-modified electrode was significantly different than the bare electrode, p-value = 0.014*, $\alpha = 0.05$.

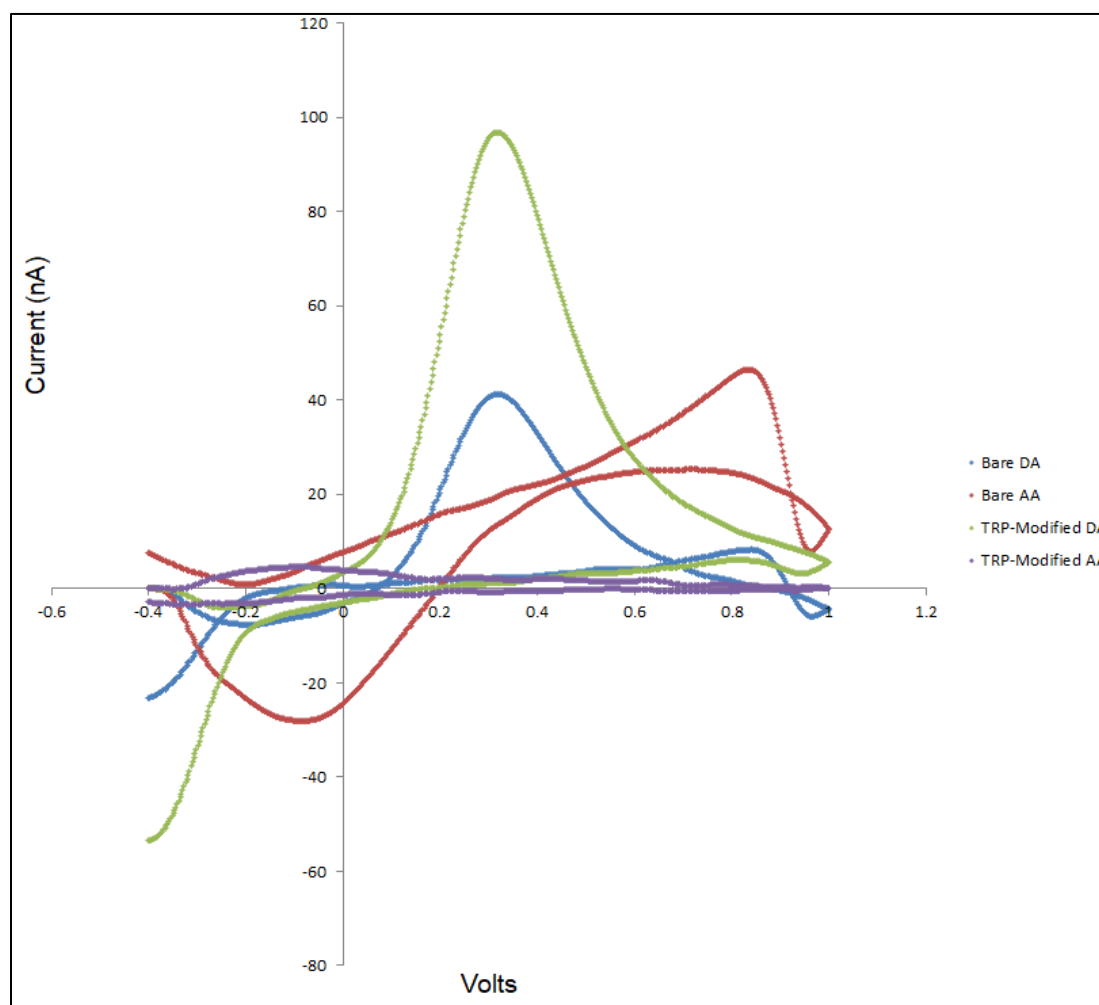


Fig 20. Background subtracted cyclic voltammograms for independent collections of DA and AA using bare and TRP-modified electrodes. TRP electrodes were modified with 1 mM TRP, scan rate = 0.02 V/s. Collections for TRP electrodes performed after extended cycling. DA – Bare, TRP modified (blue, green, respectively). AA – Bare, TRP-modified (red, purple, respectively). Collections were performed at 400 V/s, potential window: -0.4 – 1.0 V.

Chapter 4: Discussion

Electrode Modification

Cyclic Voltammograms

Previously, TRP was found to irreversibly oxidize and covalently bind in a monolayer to the surface of glassy carbon electrodes (28). Similar to the Lin and Li 2006 results, the cyclic voltammogram for TRP showed an oxidation peak in the first sweep near 0.75 V, with no reduction peak during the reverse sweep (Appendix Fig 1). Lack of a reduction peak indicated an irreversible oxidation process. Cyclic voltammograms for all experimental compounds except for 1A and 3C, failed to show evidence of an irreversible reaction with the electrode surface in a potential window of -1.7 to 1.8 V (Fig 9.) Near the ends of the -1.7 – 1.8 V potential window are peaks due to oxidation and reduction of water. Peaks occurring around this potential cannot be distinguished from water reactions, therefore, only peaks within this potential window could be attributed to the experimental compound being tested. . The cyclic voltammogram for compound 3C showed evidence of electrochemical activity based on current changes versus the negative control, however, no distinct oxidation reduction peaks could be identified. Therefore, the electrochemical behavior of 3C did not indicate an irreversible interaction with the electrode surface. Compound 1A, however, similar to TRP, was oxidized in the first sweep, and failed to reduce in the reverse sweep. Therefore, compound 1A and TRP were the only two compounds used for further testing.

Lin and Li 2006 established a monolayer surface coverage for TRP-modified electrodes by calculating the surface concentration of TRP. Modified electrodes were used in cyclic voltammetry experiments with NBu_4BF_4 , and integration under the reduction and oxidation peaks for total charge was used to calculate the number of molecules on the surface of the

electrode. This is in agreement with previous data which found 2° amines, although not as efficiently as 1° amines, to covalently bond to the surface of a carbon electrode, forming a monolayer coverage (37,38).

Position of Covalent Bonding

As discussed previously, there is disagreement in the oxidative reaction for TRP with respect to the position on TRP which binds to the surface, and how many electrons are lost in the oxidation. Lin and Li 2006 indicated binding of TRP to the carbon surface occurs at the nitrogen in the amino group of the amino acid backbone. Their proposed schematic, along with Baytak et al 2015, incorrectly depict the structure of TRP at a neutral pH. At a neutral pH, TRP is a zwitterion; the carboxyl group is deprotonated creating a negative charge and the amine group is positively charged (39). Lin and Li 2006 used XPS to confirm the presence of a C – N bond at the surface, leading to their hypothesis for binding at the amine position. However, there exists a 2° amine group in the R' group of the amino acid, which may also be the nitrogen in the C – N bond. Cyclic voltammograms for compounds 1A and 1B suggest that this is the actual position at which TRP is covalently bound to the surface.

The experimental compounds (0B, 1A, 1B, 2A, 2B, 3A, 3B, and 3C) originally tested were used due to the structural similarity to the R' group of TRP. TRP contains an indole group, whereas the experimental groups contain a benzimidazole group, with the only difference being the presence of an extra nitrogen at the 1' position of the 5-membered ring of the benzimidazole. Compounds 1A and 1B are structurally the same with the only difference being the BF₃ in complex with compound 1B at the 3' nitrogen in the 5-membered ring. Based on cyclic voltammograms for 1A and 1B, 1A covalently bound to the carbon surface (with a similar multi-cycle pattern to TRP) whereas 1B did not (Fig 9). Modification of the surface via compound 1A

was further justified based on a statistically significant decrease in sensitivity for DA, indicating that 1A was indeed covalently modified on the surface (Fig 17). Based on this evidence I hypothesize that covalent modification of 1A to the surface of the electrode occurs at the 3' position of the ring, since this was the only position unavailable for binding in 1B. The indole and benzimidazole both share a 3' nitrogen in their 5-membered ring, therefore, the proposed scheme for covalent modification of the carbon surface with TRP has TRP binding at the 3' nitrogen of its indole group (Fig 21).

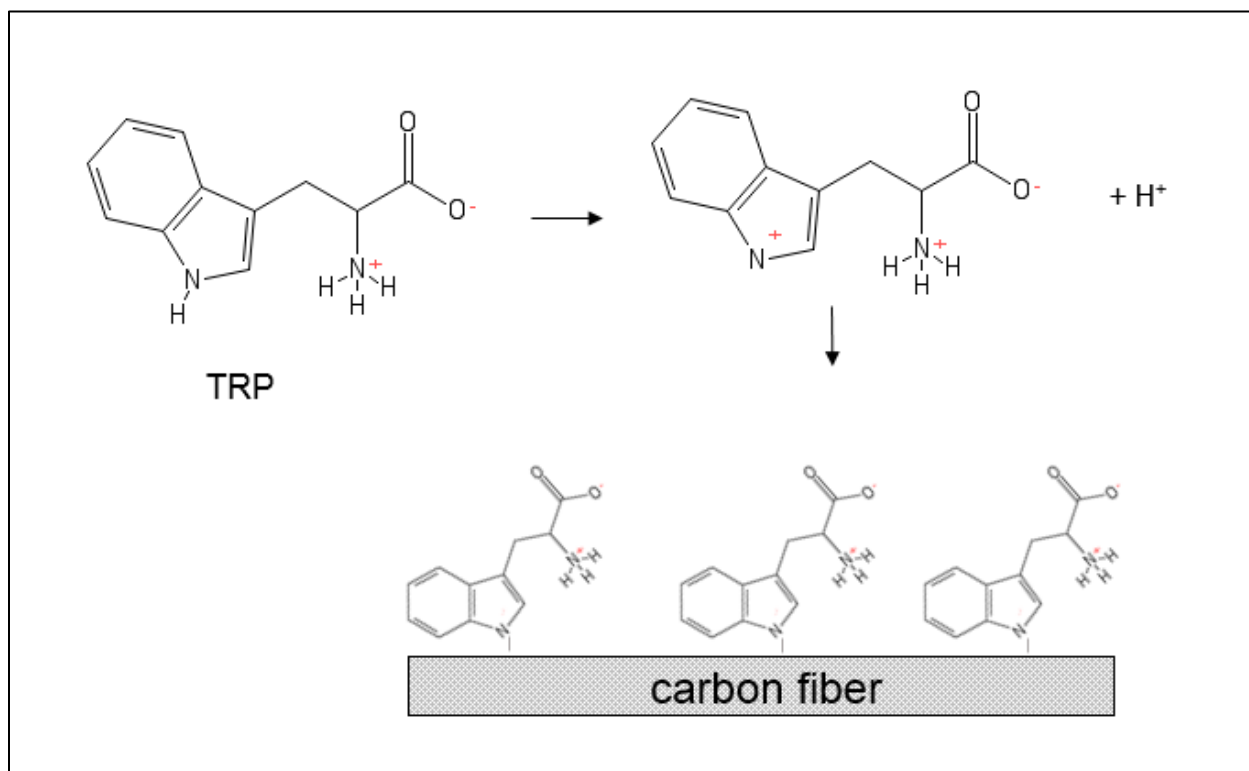


Fig 21. Proposed scheme for TRP modification of carbon fiber microelectrode surface. Covalent modification occurs between carbon and the 3' nitrogen of the indole group.

Oxidation Scheme

Baytak et al (2015) used a Tafel plot to determine their reaction scheme for TRP. They plotted $\ln(v)$ vs. anodic peak potentials (E_{ap}) and used the slope to experimentally determine the number of electrons lost in the oxidation reaction. Their Tafel plot slope indicated a loss of 2

electrons. The Tafel plot for my results yielded a slope of 0.0522, indicating a 1 electron oxidation. One possible source of the disagreement between these experiments is the use of LiClO_4 in the TRP deposition process in my current research. LiClO_4 was used by Lin and Li 2006 but its purpose was not discussed. Initial attempts at TRP modification without LiClO_4 resulted in inconsistent cyclic voltammogram results; therefore LiClO_4 was kept in the deposition procedure for my research. Based on the proposed scheme for 5-HTP in Fig. 5, LiClO_4 maybe have been responsible for preliminary oxidation of the 5'-OH group on the indole group of 5-HTP. LiClO_4 is generally used as a supporting electrolyte, therefore, it's role in the oxidative mechanism of TRP needs to be investigated further.

The position of electrochemical oxidation of TRP has not been identified. Baytak proposed a 2 electron oxidation was occurred at the 1' carbon of the 5-membered group of the indole, and a carbon in the propanoic acid group, making it a propenoic acid. My research indicates a 1 electron oxidation for TRP. The position of this oxidation has been assigned to the 3' nitrogen of the 5-membered indole ring in the scheme proposed in Fig 21. To investigate the validity of the scheme, one could perform DA detection using electrodes which were exposed to a static (no cyclic voltammetry) TRP deposition solution with and without LiClO_4 . Increased DA sensitivity can be used as a proxy for investigating the presence of TRP on the surface of the electrode. In addition, a Tafel plot for $\ln(v)$ vs. E_{ap} using TRP deposition solutions lacking LiClO_4 can help to elucidate the role of LiClO_4 in this binding mechanism.

Mechanism for Increased Sensitivity

Secondary amines are capable of covalently binding to a carbon surface. However, steric hindrance can limit binding to the surface (38). This in turn would result in a low surface concentration of TRP. A low surface concentration of TRP implies that increased sensitivity is

due primarily to an increase in electron transfer kinetics, due to the similarity in the number of active surface sites for DA adsorption. Lin and Li 2006 showed that TRP binds as a monolayer, and therefore does not provide a change in the number of binding sites for DA. One example where an increase in binding sites occurs is in the PEDOT:Nafion modified electrode (20). SEM imaging revealed a visibly thick PEDOT:Nafion coating on the electrode surface, and XPS of the surface with increasing concentrations of PEDOT in the deposition solution revealed a thicker coating; indicating a polymer layer on the electrode surface. The authors observed increased sensitivity for DA with PEDOT:Nafion modified electrodes, in addition to a loss of temporal resolution as the concentration of EDOT on the surface increased. An explanation for this observation is that the primary mechanism for increased sensitivity was not an increase in electron transfer kinetics, but an increase in DA adsorbed to the surface of the electrode. The loss in temporal resolution justifies this; time to saturation of the electrode surface takes longer if more DA is binding to the surface (40). In addition to the increased surface area of PEDOT:Nafion electrodes, they exhibited a negative charge, which increased the adsorption of DA, and repelled negatively charged interfering molecules (Fig 4.) As established in the proposed scheme for binding, TRP is a zwitterion at neutral physiological pH. Thus, there is no net charge on the electrode and the surface charge is neutral. The mechanism for TRP oxidation is not fully understood, therefore, the charge at the surface is unknown. Based on sensitivity and selectivity results, the charge on the surface is most likely negative. A negatively charged electrode would provide an explanation for the observed selectivity for DA over AA (Fig 19). This observation is discussed further in the selectivity section. To investigate the mechanism of increased sensitivity approximate surface concentrations of DA on bare electrodes and TRP-modified electrodes were calculated.

My results indicate that the surface concentration of DA is approximately 3 times greater for a TRP modified electrode. However, the negative control data in Appendix Fig 6 does not show a significant difference in DA surface concentration ratio for electrodes treated with PBS compared to electrodes that were treated with PBS, LiClO₄, and TRP (p-value = 0.091). DA surface concentration calculations were performed based on the assumption that the surface area of the electrode did not change during the deposition procedure. However, exposing carbon fiber electrodes to potentials greater than 1 V etch the electrode surface (31). The surface area calculated of the electrodes used for calculating DA surface concentration assumed a smooth, cylindrical surface. Therefore, the surface area used for calculating DA surface concentration after electrode modification may be underrepresenting the true surface area of the electrode. Possible etching of the chemical surface would result in a greater electrode surface area. Increasing the electrode surface area would decrease the DA surface concentrations calculated and thus decrease the ratios calculated and shown in Appendix Fig 6 and Fig 16. Decreasing the ratios would lead to calculated DA surface concentrations closer to concentrations calculated for the bare electrodes. There was no significant difference between the treatment and control DA surface concentrations and when assuming a smooth electrode surface after deposition. Therefore, adjusting for the assumption of a smooth electrode after deposition in theory will not show a significant difference in DA surface concentrations for treated electrodes compared to negative control electrodes. To correctly assess DA surface concentration the surface area of the electrode must not be etched during the deposition procedure. Future experiments will need to test depositing TRP in a narrow potential window not exceeding 1 V so that surface area of the electrode does not change due to etching of the electrode.

Based on the role of TRP in proteins in nature an increase in electron transfer kinetics is

expected with TRP-modified electrodes. Electron hopping across long distances in proteins via TRP residues has been established in different biological redox processes (41–44). One example of this is in a prokaryote photolyase DNA repairing mechanism (43). Wang et al. (2015) highlighted the importance of the tyrosine residue in the FAD mediated repair of the thymine-thymine dimer DNA mutation caused by UV light exposure. In addition, Wang et al. (2105) outlined the importance of the three TRP residues in the electron transfer cascade as seen in Fig 22. This TRP-residue chain is conserved in photolyases and TRP electron transfer was observed on a picosecond timescale (41,43).

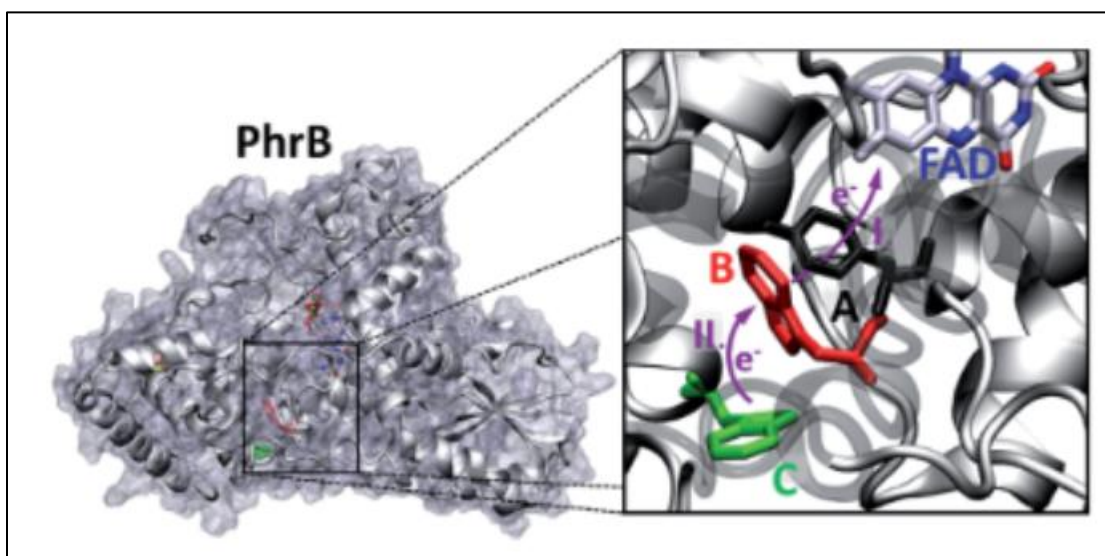


Fig 22. A, B, and C represent TRP residues in an electron transfer chain in the protein PhrB (43).

I calculated the surface area for a TRP modified electrode was calculated based on the approximate length of TRP according to binding at the secondary amine. The length was determined using experimental data provided by the pdb file 4XP1 (45). The estimated surface area for a TRP-modified electrode is 0.0196% greater than for a bare electrode. Schematic for TRP-modified surface area calculation is in Appendix Fig 3. This does not support increased surface area as the explanation for increased DA adsorption.

There is no change in oxidation potential for DA with the modified electrode, implying that the electron transfer kinetics were not sluggish, despite the increased surface concentration (Fig 20). The role of TRP in nature suggests the observed increase for DA sensitivity is due to faster electron transfer kinetics. Further work is need to determine if increased DA surface concentration is observed on TRP-modified electrodes.

Monitoring Dopamine

Sensitivity

DA collections were performed for modified electrodes before and after electrode modification, and after extended cycling of the modified electrode (Fig 17). Compound 1A resulted in a significant decrease in sensitivity for DA immediately after deposition (p-value = .028*, n=4). Due to this result, 1A was not used further for study. The significant change in DA sensitivity, however, implies that 1A had irreversibly bound to the surface, and therefore its sensitivity test serves as a proxy for showing 1A bound to the surface. The same justification is used to confirm that TRP was irreversibly bound to the surface. After extended cycling, DA sensitivity for 1A-modified electrodes was not significantly different from a bare electrode, or from the collection immediately after deposition (p-values = 0.366, 0.435, respectively, n = 4). There was general trend of increased sensitivity that potentially indicated one of two possibilities: 1A at the surface was not durable and the modified surface was degraded leading to recovered DA sensitivity, or 1A remained on the surface and extended cycling generated reactive groups on the surface leading to recovered sensitivity. The hypothesis for loss of DA sensitivity involves the structural difference between an indole (TRP) and the benzimidazole (Korich compound) groups. The benzimidazole contains a nitrogen in place of a carbon at the 1' position of the 5-membered ring. Presence of this nitrogen may affect the electron transfer mechanism

necessary for faster electron transfer kinetics required for increased DA sensitivity. If this is the case, this would further justify the argument that TRP-modified electrode sensitivity is due to faster electron transfer kinetics.

Results for TRP-modified electrodes modified with 1 mM TRP at 0.02 V/s displayed in Fig 17 shows the difference in DA sensitivity after deposition, and after extended cycling (p-values = 0.024*, 0.034* respectively, n = 4). The TRP-deposition procedure was changed with respect to scan rate and concentration to potentially improve DA sensitivity. Fig 17 shows similar results for TRP at 10 mM as there was with 1 mM TRP (scan rate of 0.02 V/s). There was a trend of increased in sensitivity for DA detection with 10 mM TRP, however, only the difference in DA sensitivity between the bare electrode and after extended cycling was significant (p-values = 0.092, 0.025*, respectively, n = 4).

ANOVA analysis of the sensitivity data for 10 mM TRP and 1 mM TRP (deposited at 0.02 V/s) were not significantly different (p-value = 1.00). This result is in agreement with the Nernstian Diffusion Response coefficients calculated for each concentration (Fig 12,13). A plot of the square of the scan rate and the peak current density can be used to determine if the reaction is diffusion controlled or adsorption controlled. If peak current density has a linear relationship with the square root of the scan rate, the reaction is diffusion controlled, and if there is a linear relationship with the scan rate, the reaction is adsorption controlled (36). There exists the possibility of having a diffusion controlled adsorption process (33). Here, a logarithmic transformation of the scan rate and the peak current density was used to evaluate this relationship. The slope of the linear fit line is indicative of the relationship; if the slope is 0.5 there is dependence with the square root of the scan rate; if the slope is 1, there is dependence with scan rate. If the slope lies in between these values, the relationship is a diffusion controlled

process where adsorption can occur. For 1 mM TRP, 10 mM TRP, and 1 mM 1A the slopes were 0.5042, 0.466, 0.4667, respectively, all indicating diffusion controlled reactions. Although the slope for 10 mM TRP was different than 1 mM TRP, it shifted to indicate a more diffusion controlled process. Thus, the lack of difference between DA sensitivity for the two methods is not surprising, since increasing the concentration did not improve the deposition process for TRP.

The effect of scan rate in deposition was also investigated for TRP-deposition. Cyclic voltammograms for 1 mM TRP and 10 mM TRP for TRP-deposition at 2 V/s displayed different patterns (Appendix Fig 2). The cyclic voltammogram for 10 mM TRP at 2 V/s best represented the same pattern of an oxidation peak in the first sweep, with the peak smaller in size in successive sweeps. Therefore, to investigate the effect of scan rate on deposition and DA sensitivity, 10 mM TRP was used. Scan rates used were 0.02 V/s and 2 V/s. The primary goal was to see if the deposition process could be performed faster, and with DEMON voltammetry software, as opposed to needing a different potentiostat capable of cyclic voltammetry at slower scan rates. There was no significant difference in DA sensitivity for electrodes modified with 10 mM TRP at 2 V/s immediately after deposition, or after extended cycling (p-values = 0.91, 0.19 respectively, $n = 4$). There is a slight trend in an increased sensitivity for DA but no statistical significant difference. At a slow scan rate (0.02 V/s), the diffusion layer grows, and because TRP is a diffusion controlled reaction, this allows for saturation of the electrode surface with TRP. The peak current density for TRP at 2 V/s is greater than at 0.02 V/s due to a decrease in the size of the diffusion layer, which is smaller because less time has elapsed for it to grow. Electrodes tested with 10 mM TRP at 2 V/s were not successfully modified, despite the shape of the cyclic voltammogram. Therefore, using fast scan rates for TRP deposition is not recommended.

A standard curve for DA sensitivity using bare and TRP-modified electrodes is shown in Fig 18. DA collections were performed after extended cycling of the TRP-modified electrodes. The 95% confidence interval for the slope determined for the bare electrode did not overlap for the slope determined for the TRP-modified electrode (slopes = 3.974×10^{-8} 5.358×10^{-9} , $7.662 \times 10^{-8} \pm 5.421 \times 10^{-9}$, respectively, $n = 5$).

Negative control data for DA sensitivity is shown in appendix Fig 4 with p-values shown in appendix Table 1. Ratios of peak DA oxidation currents were for TRP-modified electrodes over bare electrodes were used for negative control analysis. Electrodes here were modified with 1 mM TRP, scan rate = 0.02 V/s, potential window: -1.7 – 1.8 V. Electrodes treated with PBS + LiClO₄ + TRP had a significant increase in sensitivity for DA (p-value = 0.042*).

Durability

DA sensitivity for modified electrodes immediately after deposition and after extended cycling was performed to investigate the durability of the modified coating. For electrodes coated with 1 mM and 10 mM TRP at 0.02 V/s, cycling the electrodes for 10 minutes at 60 Hz and 5 minutes at 10 Hz did not significantly alter DA sensitivity compared to the sensitivity for DA immediately after deposition (p-values = 1.00, 1.00, respectively, $n = 4$). The TRP coating is stable after application of a potential waveform at high frequency. Scanning at a high frequency represents repeated use of the electrode. Cycling at 60 Hz for ten minutes is equivalent to the same number of cycles when cycling at 10 Hz for one hour. DA collections were not performed in a potential window scanning from -0.4 – 1.3 V because it has been established that potentials greater than 1 V etch the carbon layer and therefore, we would not be able to determine if sensitivity was lost due to loss of carbon or loss of TRP at the surface. XPS performed by Lin and Li 2006 revealed a stable C – N peak for 20 minutes during sonication in PBS, another

method used for removing fouling and cleaning the electrode surface. These results together support the stability of the C – N bond through methods which are used to clean the electrode surface of impurities.

In addition to extended cycling, extended DA collection was performed for 3 electrodes. Electrodes were cycled using the extended cycling conditions for the previous durability test prior to their 2 hour collection period. Sensitivity for DA was lost after 8 minutes for each electrode. The experimental design for the durability test needs to be modified in order to appropriately assess the electrodes performance over long collection periods. First, the electrode should not have been cycled prior to collection. Although this was shown not to have an effect, this may have already begun to degrade the electrode surface. Second, the 2 hour collection must be performed in dark conditions. DA is a light sensitive molecule, and should be kept from light when stored (46). DA was exposed to light during these collections, which would have degraded the molecule. The modified electrodes saw a steady decrease in DA detection for the entire remainder of the 2 hours after the 8 minute time mark. Had the TRP coating been lost on the surface, we would have expected to see a stable detection of DA similar to that of the bare electrode, but this was not the case, implying the DA had been compromised due to light exposure.

Selectivity

Selectivity for DA over other biomolecules is necessary for the proof of concept of an *in vivo* real time analytical technique specific for DA. At this time there is no standard list of biomolecules which must be investigated. A few examples of biomolecules which previous proof of concept papers have investigated are epinephrine, norepinephrine, UA, AA, dihydroxyphenylacetic acid (DOPAC), L-DOPA, and serotonin (17,20). Although most work has

been directed at improving selectivity for DA over AA and DOPAC, only AA was investigated here due to limited resources.

Results for DA and AA independent collections with bare electrodes and after extended cycling of TRP-modified electrodes are displayed in Fig 19. Electrodes were cycled using the extended cycling conditions before post modification collections as previously described. The average amperometric response ratio for DA/AA for the TRP-modified electrodes was 15 (p-value = 0.014*, n = 4). Fig 20 shows cyclic voltammograms collected for electrode 2 for independent collections of DA and AA before and after modification. An increase in DA sensitivity is observed as expected, and a significant decrease in the peak oxidation of AA is observed. Negative control data for AA detection is shown in appendix Fig 5 with corresponding p-values in appendix Table 2. Ratios of peak oxidation AA currents for TRP-modified electrodes over bare electrodes were used for the negative control analysis. Negative control data indicates a significant difference in sensitivity for AA using electrodes treated with PBS + TRP, or PBS + TRP + LiClO₄ (p-values .002*, 8.8×10^{-6} *, respectively, n = 4). The mechanism for reduced sensitivity for AA is not fully understood at this time. AA is negatively charged at physiological pH and DA is positively charged. Observed selectivity and sensitivity may be due to a negative charge on the modified-electrode surface. The negative charge would attract DA and repel AA. The oxidation mechanism for TRP deposition is not fully understood, however, these results suggest that the final charge after deposition is negative. For a complete proof of concept for the TRP-modified electrode selectivity for DOPAC will need to be assessed.

Chapter 5: Summary

My research outlines an *in vitro* proof of concept for TRP-modified electrodes for FSCV detection of the neurotransmitter DA. TRP irreversibly binds to the carbon fiber microelectrode surface via slow scan cyclic voltammetry. TRP derivatives were tested in addition to TRP for surface modification and increased sensitivity for DA. Only compound 1A covalently modified the surface of the electrode. However, 1A significantly decreased sensitivity for DA. 1A was not tested further for DA detection. This significant decrease in DA detection with 1A-modified electrodes implied that 1A was binding the surface of the electrode. As a result, compound 1A, and its analog compound 1B were used to determine the binding position for covalent modification of the surface. Compound 1B failed to bind the surface using cyclic voltammetry methods, based on the lack of an oxidation or reduction peak during a multi cycle test. 1B contains a BF_3 complex at the 3' nitrogen in its 5-membered ring, whereas 1A does not. This difference implied that the binding site for 1A must be at this nitrogen, which is not complexed in 1A. Both benzimidazole and indole groups share a 3' nitrogen in their 5-membered rings, therefore, it was hypothesized that this was the position of the C – N bond observed previously using XPS (28). It is possible that 1B was unsuccessful at modifying the surface due to reaction potentials lying outside the potential window of -1.7 – 1.8 V. Cyclic voltammetry deposition of TRP analogs such as indole are suggested for future investigation of the binding site of TRP.

Parameters for TRP-deposition were investigated for optimization of modification process. Increasing the concentration of TRP 10-fold did not improve the sensitivity of the electrode for DA. The electrode was likely saturated with 1 mM TRP, therefore no change was observed when increasing the concentration. Deposition at a faster scan rate was also tested as a method for improving the deposition process. 10 mM TRP was used for deposition at 2 V/s, a

scan rate 100-fold faster than what was originally used. Despite the shape of the cyclic voltammogram implying modification of the surface had occurred, electrodes modified at this scan rate had no significant change in DA sensitivity. TRP is a diffusion controlled reaction, and scanning at fast rates limits the growth of the diffusion layer. The peak current density is larger for 2 V/s than 0.02 V/s because the diffusion layer is smaller. Therefore, slow scan rates are recommended for TRP deposition.

Extensive cycling was performed on electrodes to investigate the durability of the C – N bond between TRP and the electrode surface. Extensive cycling for TRP deposition using 1 mM TRP at 0.02 V/s did not significantly DA sensitivity compared to collections performed immediately after deposition. Extensive cycling is used to remove fouling of the surface of electrodes. This is typically performed in a potential window scanning up to 1.3 V, however, this degrades the carbon surface. The extended cycling was performed in a potential window of -0.4 – 1.0 V, which left the carbon intact.

Selectivity for DA is critical for *in vivo* applications of modified electrodes. Amperometric response for DA and AA was recorded independently before and after electrode modification. Ratio of DA/AA current density was used to assess selectivity for DA. Average current density response was 15 times greater for DA than AA after electrode modification. Although the source of this selectivity is not understood, TRP-modified have a significantly decreased response for AA compared to DA.

These results serve as the foundation of an *in vitro* proof of concept for TRP-modified electrodes for FSCV detection of DA. TRP-modified electrodes display an increased sensitivity for DA, durability under extensive cycling, and selectivity for DA over a major interfering molecule present *in vivo*, AA.

Chapter 6: Future Directions

The oxidation mechanism during TRP deposition is not fully understood. Here, LiClO_4 was used in deposition solutions based on previous protocols for TRP-deposition (28). LiClO_4 maybe the source of disagreement in the number of electrons oxidized as experimentally determined using Tafel plots. To elucidate the mechanism, a Tafel plot for TRP deposition without LiClO_4 is recommended.

Increasing the scan rate 100-fold was unsuccessful at modifying an electrode capable of increasing sensitivity for DA due to the diffusion controlled nature of TRP deposition. Despite this, faster scan methods of a smaller range (10-fold, 2-fold), still may possess the ability to successfully modify the electrode surface. As well, 6 sweeps (3 complete cycles) were used for TRP-deposition. TRP appears to be completely oxidized after the first complete cycle, therefore, multi-cycles may not be necessary for TRP-deposition. Improving these two parameters will greatly reduce the time spent modifying electrodes.

Selectivity for DA was only tested in reference to the interfering biomolecule AA. Although there is no standard set of biomolecules to test against for a proof of concept of a modified electrode, further testing should at least be performed for DOPAC. This, along with AA, are the greatest interferences present for bare electrodes, therefore although no standard exists, these two molecules should be tested. Thus, for this *in vitro* proof of concept to be complete, selectivity for DA over DOPAC is necessary.

Moving forward, an *in vivo* proof of concept is the next step proposed for validating the use of the TRP-modified sensor. A mouse brain model is suggested for *in vivo* validation. One way to accomplish this is to use of a vibrotome to obtain striatal sections of the brain for *ex vivo*

testing. Sections of the brain treated with either DA uptake channel blockers like nomifensine, or D2-receptor antagonists such as raclopride, will be suitable for validation of DA detection (1,17). Extended collection periods, such as those performed here will also be necessary for validation of TRP-modified electrodes for acute or chronic applications.

Appendix

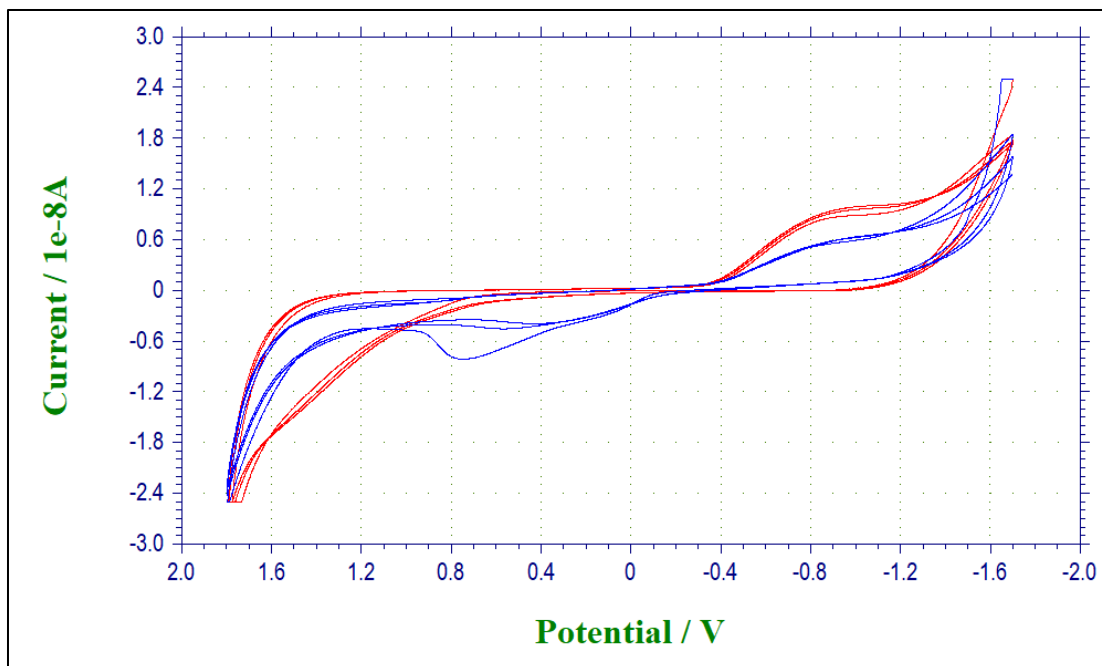


Fig 1. Cyclic voltammograms for 1 mM TRP (Blue) and negative control (red), scan rate = .02 V/s. An oxidation peak near .78 V is present in the first cycle, but not in successive cycles.

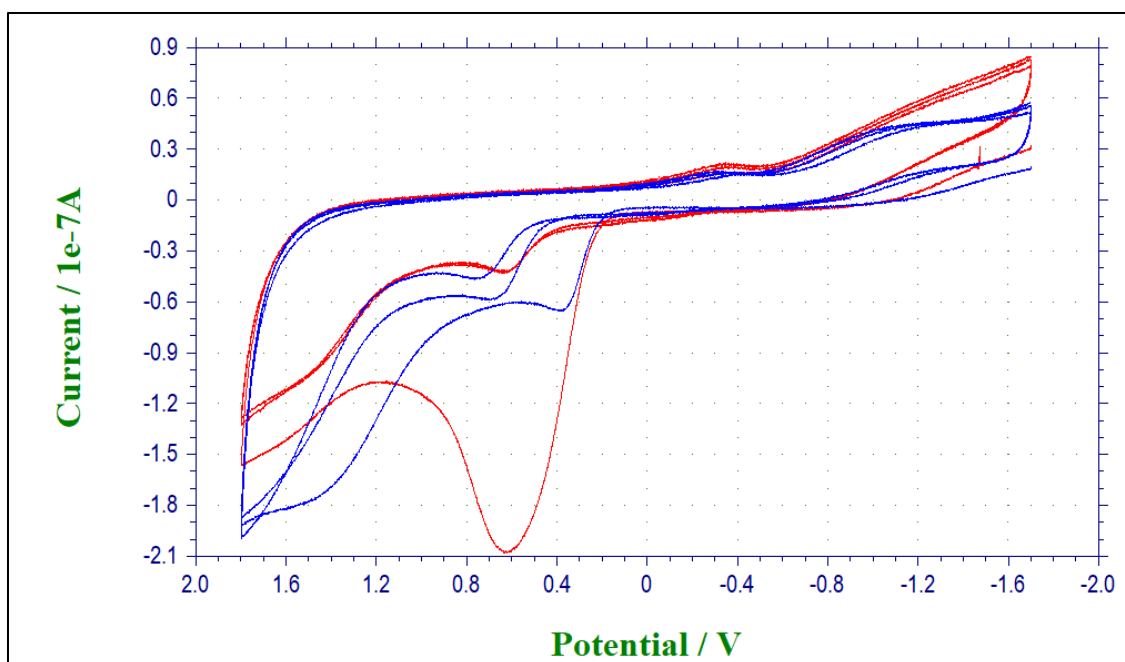


Fig 2. Cyclic voltammograms for 1 mM TRP (Blue) and 10 mM TRP (red), scan rate = 2 V/s. Largest oxidation currents were recorded in the first cycle.

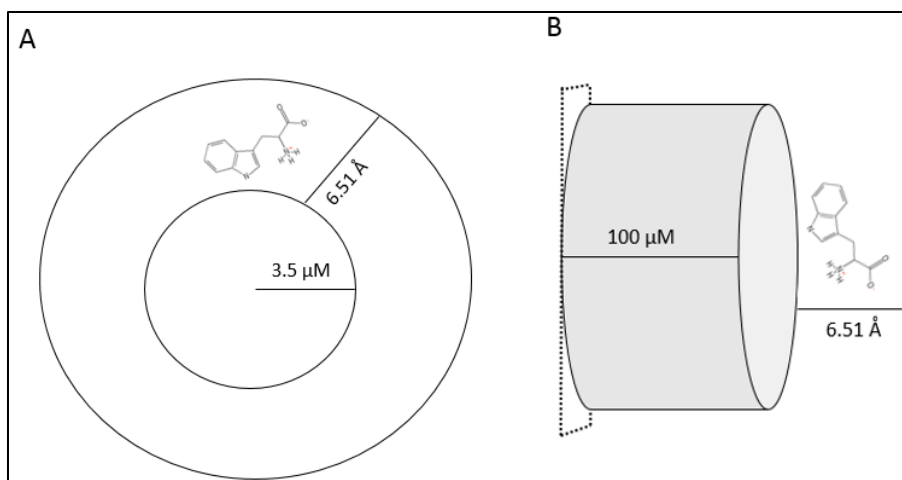


Fig 3. Schematic for determining surface area of TRP-modified electrode. Length of TRP was estimated using an experimentally derived protein structure from pdb (4XP1) and Visual Molecular Dynamics (VMD) software. A.) represents a cross section of the electrode, with the inner circle representing the carbon fiber core. B.) Represents the side profile of the electrode. Drawings are not to scale.

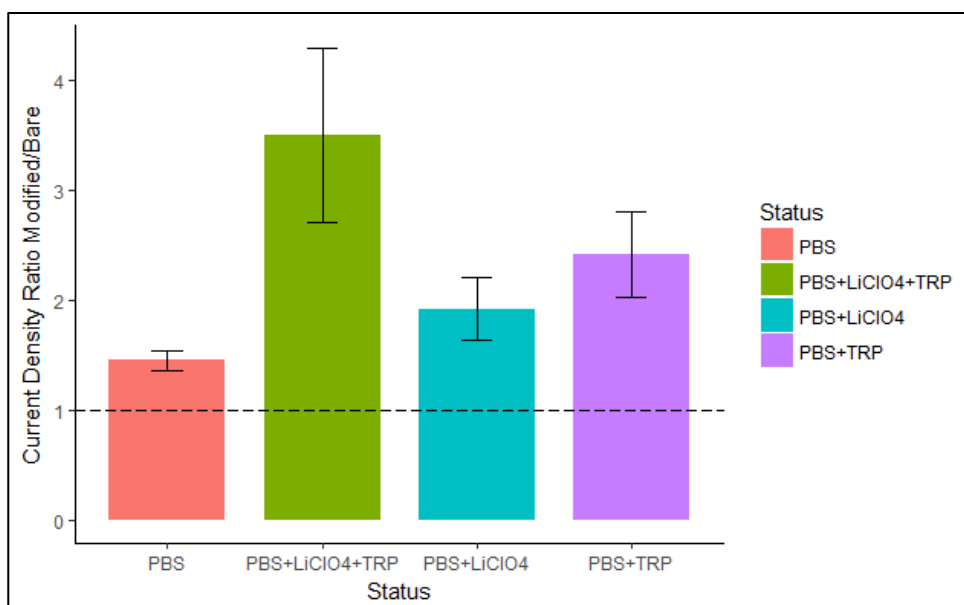


Fig 4. Negative control data for electrodes detecting 1 μM DA, using electrodes modified with 1 mM TRP and scan rate = 0.02 V/s, potential window: -1.7 – 1.8 V. Ratio of current density for DA after TRP-modification/bare electrode. PBS, treatment (PBS + TRP + LiClO₄), PBS + LiClO₄, and PBS + TRP are shown in pink, green, blue, and purple, respectively. n = 4.

PBS vs.	p-value
PBS + LiClO ₄	0.17
PBS + TRP	0.052
PBS + LiClO ₄ + TRP	0.042*

Table 1. p-values for negative control data shown in appendix Fig 4. * indicates significant difference, $\alpha = 0.05$.

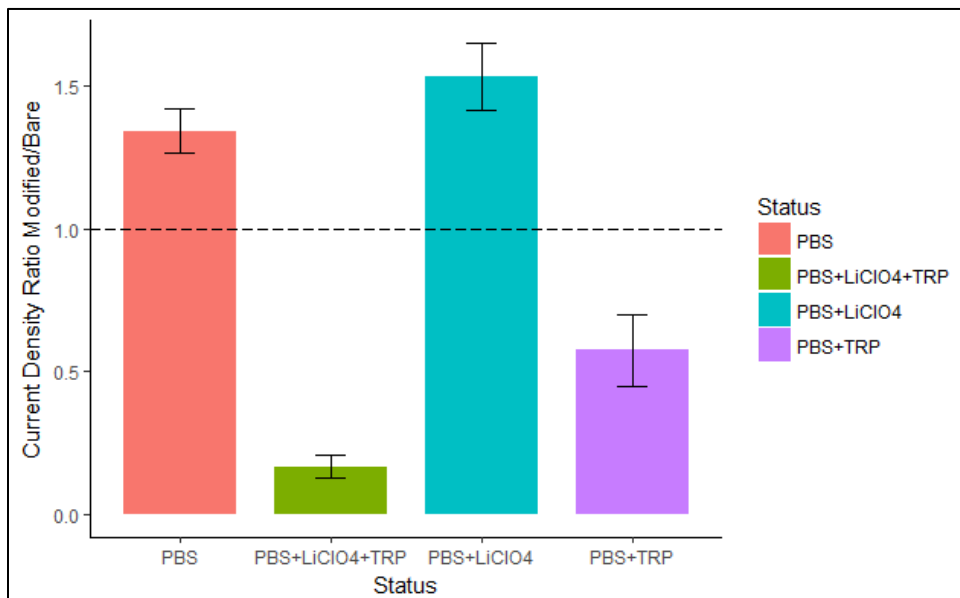


Fig 5. Negative control data for electrodes detecting 200 μ M AA, using electrodes modified with 1 mM TRP and scan rate = 0.02 V/s, potential window: -1.7 – 1.8 V. Ratio of current density for AA after TRP-modification/bare electrode. PBS, treatment (PBS + TRP + LiClO₄), PBS + LiClO₄, and PBS + TRP are shown in pink, green, blue, and purple, respectively. n = 4.

PBS vs.	p-value
PBS + LiClO ₄	0.22
PBS + TRP	0.002*
PBS + LiClO ₄ + TRP	8.8×10^{-6} *

Table 2. p-values for negative control data shown in appendix Fig 5. * indicates significant difference, $\alpha = 0.05$.

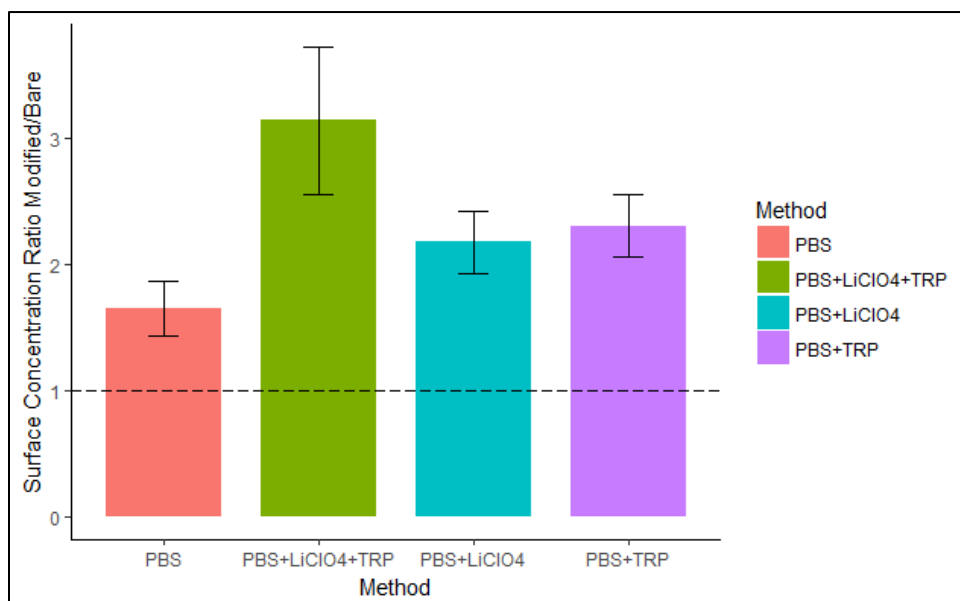


Fig 6. Negative control data for electrodes DA surface concentration using electrodes modified with 1 mM TRP and scan rate = 0.02 V/s, potential window: -1.7 – 1.8 V. Ratio of DA surface concentration (mol/cm²) after TRP-modification/bare electrode. PBS, treatment (PBS + TRP + LiClO₄), PBS + LiClO₄, and PBS + TRP are shown in pink, green, blue, and purple, respectively. n = 4.

PBS vs.	p-value
PBS + LiClO ₄	0.091
PBS + TRP	0.19
PBS + LiClO ₄ +TRP	0.12

Table 3. p-values for negative control data shown in appendix Fig 6. * indicates significant difference, $\alpha = 0.05$.

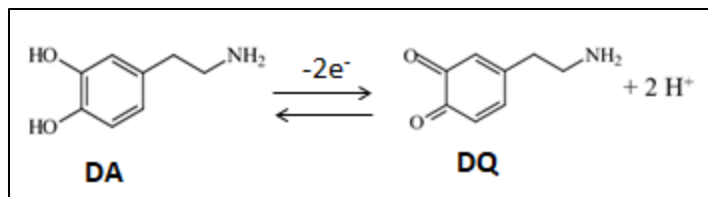


Fig 7. Dopamine (DA) cyclic oxidation to dopamine-o-quinone (DQ), and reduction back to DA.

References

1. Schwerdt HN, Shimazu H, Amemori K-I, Amemori S, Tierney PL, Gibson DJ, et al. Long-term dopamine neurochemical monitoring in primates. *Proc Natl Acad Sci U S A*. 2017 Dec 12;114(50):13260–13265.
2. Björklund A, Dunnett SB. Dopamine neuron systems in the brain: an update. *Trends Neurosci*. 2007 May;30(5):194–202.
3. Sennvik K, Fastbom J, Blomberg M, Wahlund LO, Winblad B, Benedikz E. Levels of alpha- and beta-secretase cleaved amyloid precursor protein in the cerebrospinal fluid of Alzheimer's disease patients. *Neurosci Lett*. 2000 Jan 14;278(3):169–172.
4. Lees AJ, Hardy J, Revesz T. Parkinson's disease. *The Lancet*. 2009 Jun 13;373(9680):2055–2066.
5. Guzmán-Ramos K, Moreno-Castilla P, Castro-Cruz M, McGaugh JL, Martínez-Coria H, LaFerla FM, et al. Restoration of dopamine release deficits during object recognition memory acquisition attenuates cognitive impairment in a triple transgenic mice model of Alzheimer's disease. *Learn Mem*. 2012 Sep 14;19(10):453–460.
6. Corvol J-C, Bonnet C, Charbonnier-Beaupel F, Bonnet A-M, Fiévet M-H, Bellanger A, et al. The COMT Val158Met polymorphism affects the response to entacapone in Parkinson's disease: a randomized crossover clinical trial. *Ann Neurol*. 2011 Jan;69(1):111–118.
7. Robinson DL, Venton BJ, Heien MLAV, Wightman RM. Detecting subsecond dopamine release with fast-scan cyclic voltammetry in vivo. *Clin Chem*. 2003 Oct;49(10):1763–1773.
8. Ramsson ES, Cholger D, Dionise A, Poirier N, Andrus A, Curtiss R. Characterization of Fast-Scan Cyclic Voltammetric Electrodes Using Paraffin as an Effective Sealant with In Vitro and In Vivo Applications. *PLoS ONE*. 2015 Oct 27;10(10):e0141340.
9. Zhang Y, Wang B, Wan H, Zhou Q, Li T. Meta-analysis of the insulin degrading enzyme polymorphisms and susceptibility to Alzheimer's disease. *Neurosci Lett*. 2013 Apr 29;541:132–137.
10. Jaquins-Gerstl A, Michael AC. A review of the effects of FSCV and microdialysis measurements on dopamine release in the surrounding tissue. *Analyst (Lond)*. 2015 Jun 7;140(11):3696–3708.
11. Atcherley CW, Laude ND, Parent KL, Heien ML. Fast-scan controlled-adsorption voltammetry for the quantification of absolute concentrations and adsorption dynamics. *Langmuir*. 2013 Dec 3;29(48):14885–14892.
12. Gottås A, Ripel Å, Boix F, Vindenes V, Mørland J, Øiestad EL. Determination of dopamine concentrations in brain extracellular fluid using microdialysis with short

- sampling intervals, analyzed by ultra high performance liquid chromatography tandem mass spectrometry. *J Pharmacol Toxicol Methods*. 2015 Aug;74:75–79.
13. Keithley RB, Takmakov P, Bucher ES, Belle AM, Owesson-White CA, Park J, et al. Higher sensitivity dopamine measurements with faster-scan cyclic voltammetry. *Anal Chem*. 2011 May 1;83(9):3563–3571.
 14. Bennet KE, Tomshine JR, Min H-K, Manciu FS, Marsh MP, Paek SB, et al. A Diamond-Based Electrode for Detection of Neurochemicals in the Human Brain. *Front Hum Neurosci*. 2016 Mar 15;10:102.
 15. Hanifah SA, Heng LY, Ahmad M. Biosensors for phenolic compounds by immobilization of tyrosinase in photocurable methacrylic-acrylic membranes of varying hydrophilicities. *Anal Sci*. 2009 Jun;25(6):779–784.
 16. Eisenhofer G, Tian H, Holmes C, Matsunaga J, Roffler-Tarlov S, Hearing VJ. Tyrosinase: a developmentally specific major determinant of peripheral dopamine. *FASEB J*. 2003 Jul;17(10):1248–1255.
 17. Njagi J, Chernov MM, Leiter JC, Andreescu S. Amperometric detection of dopamine in vivo with an enzyme based carbon fiber microbiosensor. *Anal Chem*. 2010 Feb 1;82(3):989–996.
 18. Njagi J, Ispas C, Andreescu S. Mixed ceria-based metal oxides biosensor for operation in oxygen restrictive environments. *Anal Chem*. 2008 Oct 1;80(19):7266–7274.
 19. Malmo J, Sandvig A, Vårum KM, Strand SP. Nanoparticle mediated P-glycoprotein silencing for improved drug delivery across the blood-brain barrier: a siRNA-chitosan approach. *PLoS ONE*. 2013 Jan 23;8(1):e54182.
 20. Vreeland RF, Atcherley CW, Russell WS, Xie JY, Lu D, Laude ND, et al. Biocompatible PEDOT:Nafion composite electrode coatings for selective detection of neurotransmitters in vivo. *Anal Chem*. 2015 Mar 3;87(5):2600–2607.
 21. Wiedemann DJ, Basse-Tomusk A, Wilson RL, Rebec GV, Wightman RM. Interference by DOPAC and ascorbate during attempts to measure drug-induced changes in neostriatal dopamine with Nafion-coated, carbon-fiber electrodes. *J Neurosci Methods*. 1990 Oct;35(1):9–18.
 22. Taylor IM, Robbins EM, Catt KA, Cody PA, Happe CL, Cui XT. Enhanced dopamine detection sensitivity by PEDOT/graphene oxide coating on in vivo carbon fiber electrodes. *Biosens Bioelectron*. 2017 Mar 15;89(Pt 1):400–410.
 23. Winkler JR, Gray HB. Could tyrosine and tryptophan serve multiple roles in biological redox processes? *Philos Transact A Math Phys Eng Sci*. 2015 Mar 13;373(2037).
 24. Monni R, Al Haddad A, van Mourik F, Auböck G, Chergui M. Tryptophan-to-heme electron transfer in ferrous myoglobins. *Proc Natl Acad Sci U S A*. 2015 May 5;112(18):5602–5606.

25. Black KM, Clark-Lewis I, Wallace CJ. Conserved tryptophan in cytochrome c: importance of the unique side-chain features of the indole moiety. *Biochem J.* 2001 Nov 1;359(Pt 3):715–720.
26. Field MJ, Bains RK, Warren JJ. Using an artificial tryptophan “wire” in cytochrome c peroxidase for oxidation of organic substrates. *Dalton Trans.* 2017 Aug 22;46(33):11078–11083.
27. Li Y, Huang X, Chen Y, Wang L, Lin X. Simultaneous determination of dopamine and serotonin by use of covalent modification of 5-hydroxytryptophan on glassy carbon electrode. *Microchim Acta.* 2009 Jan;164(1-2):107–112.
28. Lin X, Li Y. Monolayer covalent modification of 5-hydroxytryptophan on glassy carbon electrodes for simultaneous determination of uric acid and ascorbic acid. *Electrochim Acta.* 2006 Aug;51(26):5794–5801.
29. Baytak AK, Aslanoglu M. Voltammetric quantification of tryptophan using a MWCNT modified GCE decorated with electrochemically produced nanoparticles of nickel. *Sensors and Actuators B: Chemical.* 2015 Dec;220:1161–1168.
30. Ramsson ES. A pipette-based calibration system for fast-scan cyclic voltammetry with fast response times. *BioTechniques.* 2016 Nov 1;61(5):269–271.
31. Takmakov P, Zachek MK, Keithley RB, Walsh PL, Donley C, McCarty GS, et al. Carbon microelectrodes with a renewable surface. *Anal Chem.* 2010 Mar 1;82(5):2020–2028.
32. Roberts JG, Moody BP, McCarty GS, Sombers LA. Specific oxygen-containing functional groups on the carbon surface underlie an enhanced sensitivity to dopamine at electrochemically pretreated carbon fiber microelectrodes. *Langmuir.* 2010 Jun 1;26(11):9116–9122.
33. Alghamdi AF. Voltammetric analysis of montelukast sodium in commercial tablet and biological samples using the hanging mercury drop electrode. *Port Electrochim Acta.* 2014;32(1):51–64.
34. Hermans A, Seipel AT, Miller CE, Wightman RM. Carbon-fiber microelectrodes modified with 4-sulfobenzene have increased sensitivity and selectivity for catecholamines. *Langmuir.* 2006 Feb 28;22(5):1964–1969.
35. Singleton ST, O’Dea JJ, Osteryoung J. Analytical utility of cylindrical microelectrodes. *Anal Chem.* 1989 Jun;61(11):1211–1215.
36. Wang J. *Analytical Electrochemistry.* New York, USA: John Wiley & Sons, Inc.; 2000.
37. Deinhammer RS, Ho M, Anderegge JW, Porter MD. Electrochemical oxidation of amine-containing compounds: a route to the surface modification of glassy carbon electrodes. *Langmuir.* 1994 Apr;10(4):1306–1313.

38. Downard AJ. Electrochemically Assisted Covalent Modification of Carbon Electrodes. *Electroanalysis*. 2000 Oct 1;
39. Tryptophan | C₁₁H₁₂N₂O₂ - PubChem [Internet]. [cited 2018 Mar 2]. Available from: <https://pubchem.ncbi.nlm.nih.gov/compound/L-tryptophan#section=Ecological-Information>
40. Strand AM, Venton BJ. Flame etching enhances the sensitivity of carbon-fiber microelectrodes. *Anal Chem*. 2008 May 15;80(10):3708–3715.
41. Takematsu K, Williamson H, Blanco-Rodríguez AM, Sokolová L, Nikolovski P, Kaiser JT, et al. Tryptophan-accelerated electron flow across a protein-protein interface. *J Am Chem Soc*. 2013 Oct 16;135(41):15515–15525.
42. Byrdin M, Villette S, Eker APM, Brettel K. Observation of an intermediate tryptophanyl radical in W306F mutant DNA photolyase from *Escherichia coli* supports electron hopping along the triple tryptophan chain. *Biochemistry*. 2007 Sep 4;46(35):10072–10077.
43. Holub D, Ma H, Krauß N, Lamparter T, Elstner M, Gillet N. Functional role of an unusual tyrosine residue in the electron transfer chain of a prokaryotic (6–4) photolyase. *Chem Sci*. 2018;9(5):1259–1272.
44. Lukacs A, Eker APM, Byrdin M, Brettel K, Vos MH. Electron hopping through the 15 Å triple tryptophan molecular wire in DNA photolyase occurs within 30 ps. *J Am Chem Soc*. 2008 Nov 5;130(44):14394–14395.
45. Wang KH, Penmatsa A, Gouaux E. Neurotransmitter and psychostimulant recognition by the dopamine transporter. *Nature*. 2015 May 21;521(7552):322–327.
46. Ghanayem NS, Yee L, Nelson T, Wong S, Gordon JB, Marcante K, et al. Stability of dopamine and epinephrine solutions up to 84 hours. *Pediatr Crit Care Med*. 2001 Oct;2(4):315–317.